ISME

The Iranian Journal of Mechanical Engineering Transactions of ISME
Journal homepage: https://jmee.isme.ir/
Vol. 26, No. 1, 2025, pp. 130-161

Research Paper

DOI: https://doi.org/10.30506/jmee.2024.2037135.1351

Geometry Improvement of an Asymmetric S-shaped Intake with a Combination of Artificial Neural Networks and Genetic Algorithm

Asghar Fazli[*]
M.Sc. Student

Mohammad Mostafa Mahmoodi[†]
Professor

The air intake duct provides the required air for the engine under various aircraft operating conditions. Therefore, designing an intake duct with minimum total pressure loss and maximum flow uniformity is of great importance. Non-uniform flow entering the engine leads to performance degradation and, in severe cases, can even cause surge and engine failure. In the present research, an asymmetric S-shaped air intake duct is optimized to reduce total pressure loss and flow distortion at the exit plane. The optimization process uses a genetic algorithm and an artificial neural network. It includes geometry modeling, mesh generation, three-dimensional simulations, database preparation, neural network training, and genetic algorithm optimization. The genetic algorithm uses the neural network to evaluate the objective function and identify the optimal geometry. A comparison of the optimized results with the baseline geometry shows a reduction of over 74% in flow distortion and over 16% in total pressure loss.

Keywords: Geometry improvement, S-shaped intake, Artificial neural networks, Genetic algorithm

1 Introduction

A critical issue is designing an intake duct that reduces flow velocity while minimizing total pressure loss and outlet flow distortion and providing the required air mass flow rate to the engine. The appropriate geometry for an engine inlet duct depends not only on the engine itself and its performance characteristics but also on factors such as the aircraft mission profile, the engine's location on the airframe or wing, the take-off and landing environment, and the operational requirements that determine the aircraft's critical maneuvers.

[*]MSc. Air Research Center, Air Industry Org, Tehran, Iran, asgharf680@gmail.com
[†]Corresponding author, Associate Professor, Faculty of Aerospace, Malek Ashtar University of Technology, Iran mostafamahmoodi@mut.ac.ir

Received: 2024/07/30, Revised: 2024/09/26, Accepted: 2024/12/10

Therefore, the optimum intake duct geometry varies according to these factors, affecting both the centerline shape and the cross-sectional profiles along the duct.
On the other hand, flow uniformity and total pressure loss within the intake duct are complex functions of the inlet flow characteristics and the duct geometry, which cannot be evaluated mathematically (their solution requires solving the complex Navier-Stokes equations, which do not have analytical solutions due to their complexity). Hence, three-dimensional simulations must be conducted to assess the intake duct's performance, and the optimized geometry must be experimentally validated in a wind tunnel. Over the years, numerous studies have been conducted to investigate the flow behavior in intake ducts and optimize their geometry. In general, these studies can be categorized into experimental and computational research.
In a recent experimental study by Weske[1], various cross-sections of a curved duct were examined to determine the effect of the centerline curve and the ratio of the inlet to outlet radius on the total pressure drop. The study included circular and elliptical cross-sections, with the flow subjected to velocities ranging from 100 to 300 feet per second. These experiments showed that the centerline curve and the ratio of the inlet to outlet radius significantly affected the total pressure loss. In 1993, Wellborn [2] conducted experiments on compressible flow through an S-shaped duct. The experimental results were analyzed, and pressure and velocity distributions were calculated at various duct sections. This study provided substantial data on aerodynamic parameters and the flow separation mechanism, which is crucial for the computational validation of S-duct simulations. Thanks to the advancements and increased speed of computational systems, it is now possible to accurately predict fluid behavior through computational fluid dynamics (CFD) and three-dimensional simulations.
Delot and Scharnhorst [3] have conducted significant studies on the same geometry as Wellborn's experiments. This study explores different turbulence models, mesh configurations, and solver codes to obtain a numerical model that closely aligns with the experimental results.
Fiola and Agarwal [4] conducted experiments using the FLUENT software, testing four different turbulence models. Their findings indicated that the SST k-ω model was the most effective in predicting the total pressure loss along the centerline.
Numerous studies have been published in the field of intake duct optimization [5-10]. Parhrizkar etal. [11] modeled and solved the three-dimensional flow inside an S-shaped intake for two different center lines. They found that reducing the center line curvature resulted in increased pressure recovery. Furlan et al.[12] studied the flow inside a rectangular duct to minimize total pressure loss and maximize flow uniformity. They significantly improved pressure recovery and flow uniformity by 58% and 54%, respectively. Tridello[13] conducted a study to reduce total pressure loss by optimizing a circular intake duct. Rigobello [14] performed a multi-objective optimization on an S-shaped duct to achieve the best pressure recovery and minimum flow distortion. As a result of this optimization, pressure recovery improved by 19%, and flow distortion decreased by 13%. The geometry parameterization was performed using the Free Form Deformation (FFD) method. Chiereghin et al.[15] used a similar approach to enhance the performance of an intake duct, which led to a noteworthy 20% reduction in total pressure loss and a 10% decrease in flow distortion. D'Ambros et al. [16]used the FFD method to optimize an intake duct to reduce the exit flow angle and increase pressure recovery. The evaluation of the optimized geometry using CFD showed that the optimized geometry reduced the pressure drop by 14% and the exit flow angle by 70%. Gan and Zhang [17] used a multi-objective optimization strategy to improve the performance of an S-shaped intake. This study redesigned the centerline and cross-sectional shapes to prevent excessive flow expansion within the duct. The results of the optimized geometry showed a 3.16% reduction in flow distortion and a 1.1% increase in pressure recovery. Alberto Meneghin [18]investigated the relationship between inlet duct optimization and compressor performance. To this end, he re-evaluated previous optimizations with different objectives, such as improving

pressure recovery, reducing flow distortion, and reducing pressure drag, while considering the engine performance and simultaneously simulating the three-dimensional flow.Kamat et al. [19]employed an adjoint method to optimize an S-shaped intake duct for distortion reduction. This optimization resulted in a 2.15% reduction in intake distortion. Madadi et al.[20] worked on optimizing an S-shaped duct aiming to reduce the total pressure loss and flow distortion, which led to a 32.5% improvement in pressure recovery and a 35.8% reduction in distortion. Since the flow's distortion and total pressure loss cannot be mathematically evaluated as a function of geometry, direct conventional methods cannot be used to obtain the optimal geometry either. On the other hand, while the three-dimensional flow solution is faster and cheaper compared to wind tunnel testing, it still incurs significant computational cost and time. Based on the above, implementing an optimization process for the engine intake duct, where distortion and total pressure loss can be evaluated while limiting the number of 3D solutions, can accelerate the optimization process and reduce its costs.

In the present study, a genetic algorithm is employed for the multi-objective optimization of an asymmetric S-shaped intake air duct. Although this method requires repeated evaluation of the objective function, direct implementation is not justifiable in terms of time cost due to the time-consuming evaluation for this specific problem. Therefore, an artificial neural network is used as a surrogate function to call within the genetic algorithm optimization process.

2 Methodology

2. 1 Geometry of the studied air inlet duct

The studied geometry is shown in Figure (1). The geometric dimensions are in millimeters. The air inlet duct has an S-shape, and the cross-sectional area is constant at the inlet and outlet sections.

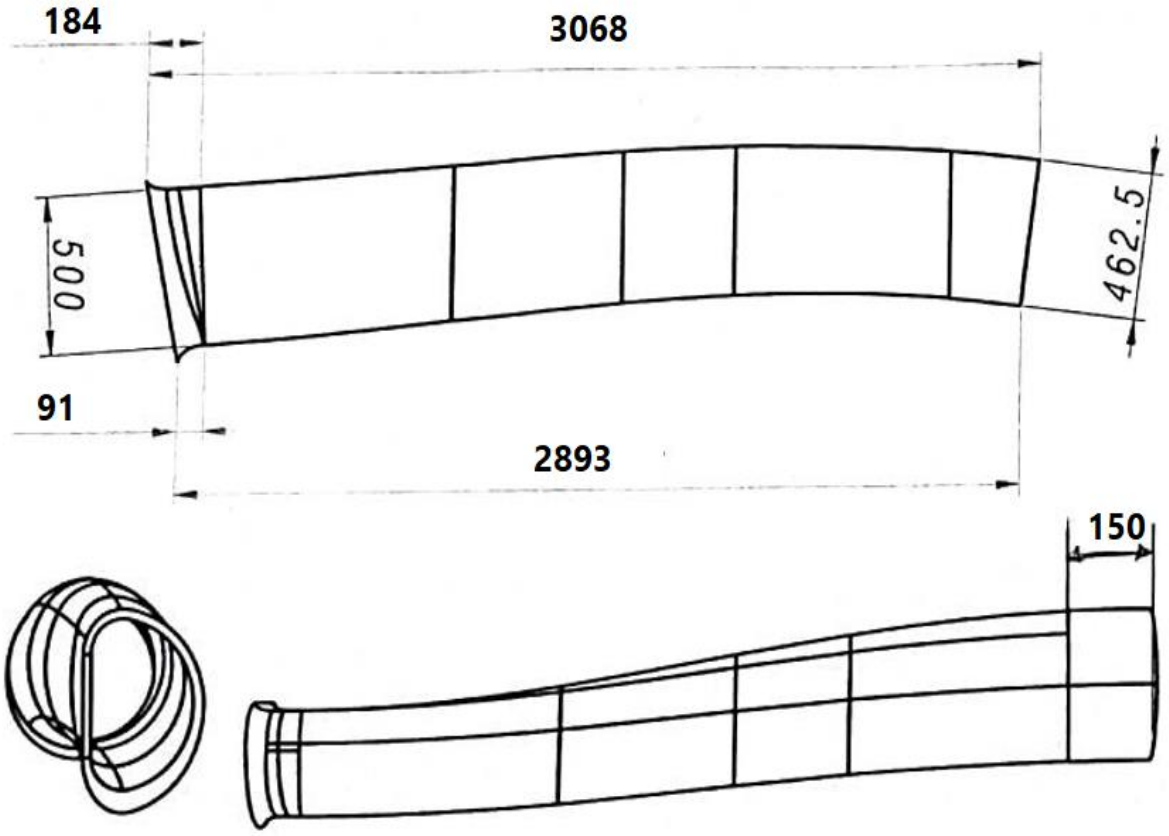

Figure 1 The geometry of the studied intake duct

2.2 Calculation of objective functions

This project aims to optimize an S-shaped intake duct to deliver airflow to the engine with minimum total pressure loss and maximum flow uniformity (minimum distortion). In this process, we seek a method to achieve the best geometry with minimum total pressure loss and flow uniformity while requiring fewer 3D solutions.
Since the flow within the duct is inherently nonlinear and the governing equations are highly complex, it is almost impossible to predict the flow behavior in response to geometry changes using analytical methods. Addressing each individual geometry by solving the governing flow equations and applying computational fluid dynamics methods to assess the results is essential. Additionally, due to the nonlinear nature of the governing flow equations, the objective function distribution is irregular and has many local minima. This increases the risk of the optimization process becoming trapped in local minima, thus failing to find the global optimum.
These two considerations add complexity to the process of finding an optimal solution. The innovation of this research lies in proposing a method to address these complexities for optimizing the engine inlet geometry.
To achieve the first goal (finding the optimal geometry while avoiding local minima), a genetic algorithm, which is a metaheuristic optimization method for nonlinear problems, has been employed. For the second goal (reducing the number of 3D flow solutions), a neural network has been employed due to its powerful learning capability to tackle nonlinear problems by identifying the nonlinear relationships between the inputs and outputs, independent of the physical nature of the problem.

2.2.1 Total pressure loss calculation

The total pressure loss is obtained from Equation (2):

$$PR = \frac{P_{o,out}}{P_{o,in}} \tag{1}$$

$$\Delta P = 1 - PR \tag{2}$$

In Equation (1), PR is the total pressure recovery, and Po, out, and Po, in are the total pressures at the air inlet duct outlet and inlet, respectively.

2.2.2 Flow distortion calculation

The flow distortion is defined by Equation (3):

$$DC_{60} = \frac{P_{60}}{q_f} \tag{3}$$

Where qf is the average dynamic head at the air inlet duct exit plane, and P60 is calculated as follows:

$$P_{60} = max\left(abs\left(P_a - P_f\right)\right) \tag{4}$$

Here, Pf is the average total pressure at the air inlet duct exit plane, and Pa is the average total pressure in an arbitrarily selected 60-degree sector of the exit plane.

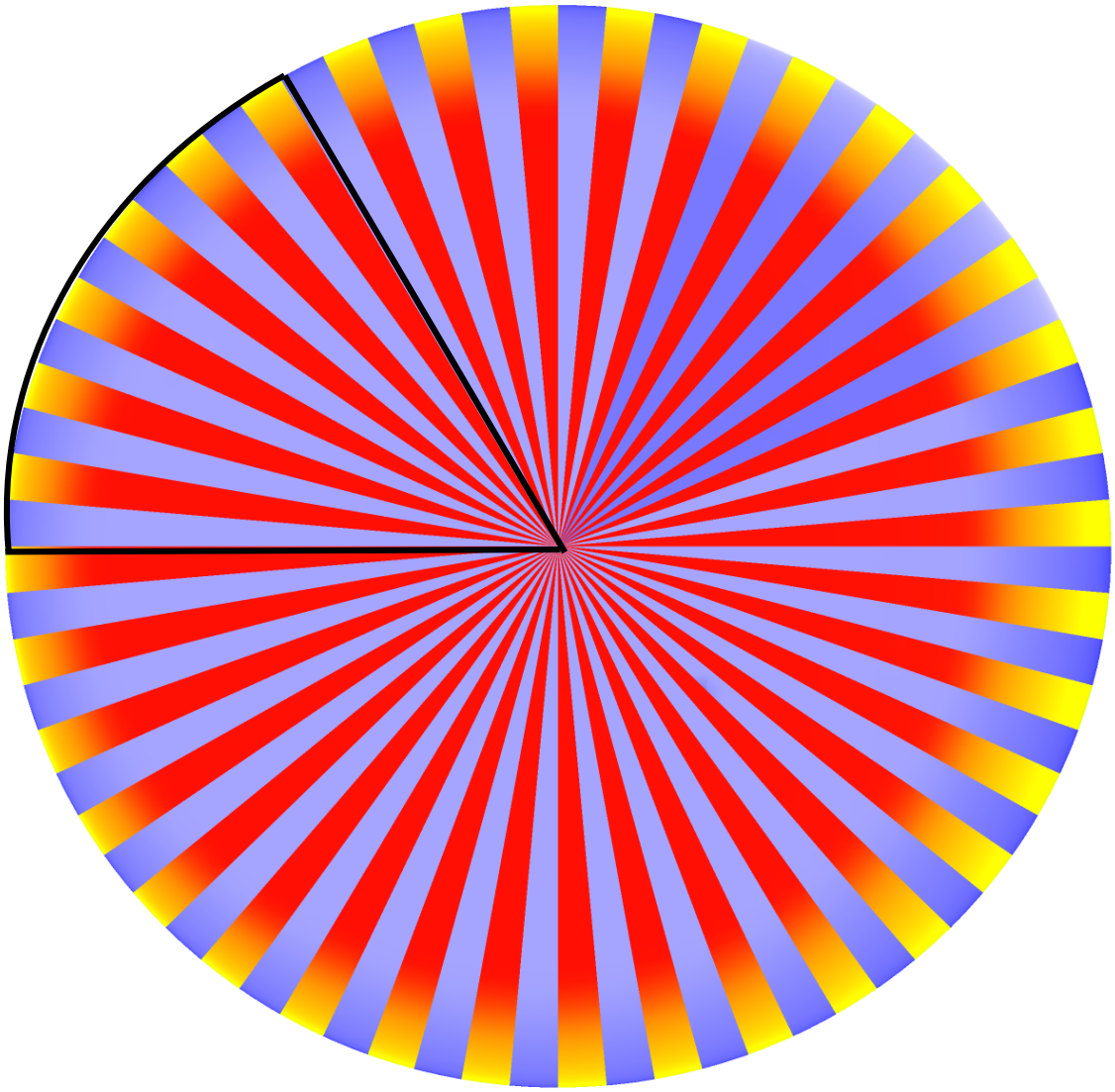

Figure 2 The 60-degree sectors for defining the exit flow distortion

2.2.3 Calculation of the final objective function

The ultimate goal is the simultaneous reduction of flow distortion and total pressure loss. Since both these parameters need to be minimized, we define the objective function as the sum of these two parameters (Equation (5)), and the optimization is performed to minimize this objective function. We trained a separate neural network for each component of the objective function (pressure drop and flow distortion). Therefore, to compute the objective function using the input geometry, we first calculate the flow distortion and pressure drop by invoking the corresponding neural networks and then compute the objective function by summing them up.

$$Target\ Parameter = \Delta P + DC60 \tag{5}$$

Due to the nature of the problem at hand, there are numerous local minima that we may get trapped in during the optimization process. In general, for optimization problems, the use of the genetic algorithm method is a common and suitable approach to escape local minima. The genetic algorithm is an efficient metaheuristic method widely used in location problems. This algorithm is particularly suitable for problems involving a vast state space, where examining all states in higher dimensions is practically impossible. A notable feature of this method is its high speed in moving toward the solution.

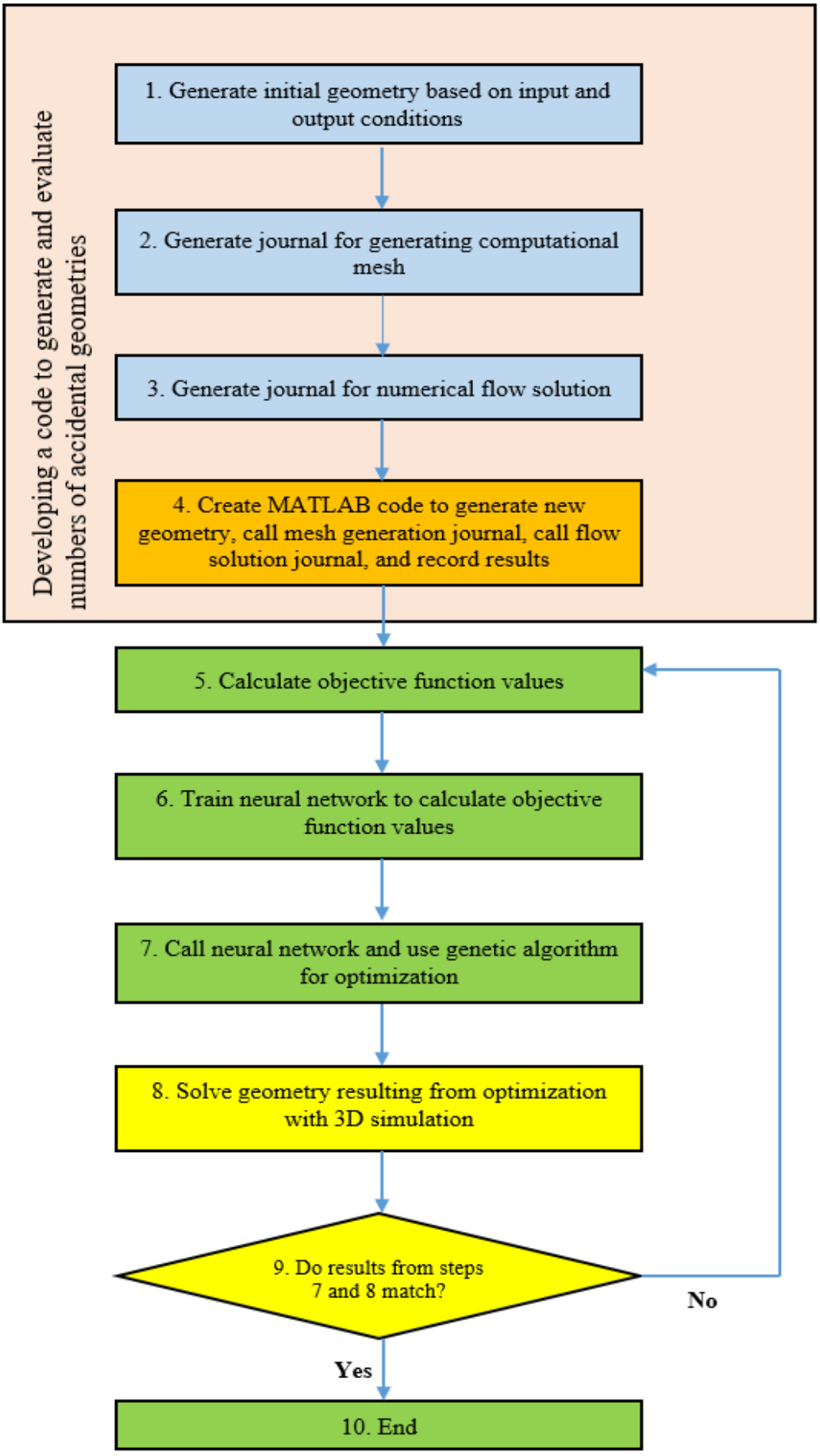

Figure 3 The optimization process of the inlet geometry in the present study

However, it should be noted that the genetic algorithm requires a large number of objective function evaluations. If the geometry estimated by the genetic algorithm needs to be evaluated through a 3D flow solution each time, the optimization process will be extremely time-consuming, costly, and unjustifiable. Therefore, using an artificial neural network is a method that can accelerate the computations. Although the process of training a neural network is time-consuming, it is much more justifiable and less time-consuming compared to the time required for a 3D flow solution within the duct. Secondly, once the neural network is trained, its use is very fast and user-friendly. Consequently, in the present study, computational fluid dynamics simulations are performed to evaluate a limited number (55) of initial geometries randomly generated based on the baseline geometry. It should be noted that by imposing constraints on the generation of initial geometries, the consideration of geometries that are clearly unsuitable from the outset should be prevented. After solving these geometries and evaluating the objective function values, the initial database required for training the neural network is obtained. At this stage, using this database, the neural networks are trained to calculate the objective functions based on the input geometry.

Now, the trained neural network is available as a ready-made module that can calculate the objective function values for any input geometry, serving the genetic algorithm. The genetic algorithm utilizes the neural network to call and evaluate the objective function, ultimately proposing an optimized geometry.

The geometry selected by the genetic algorithm will need to be evaluated through a three-dimensional simulation. If the simulation output matches the neural network output, then this geometry will be considered the optimal solution. The result of the three-dimensional solution is incorporated into the database, and the neural network undergoes retraining. This iterative process is continued until the genetic algorithm's objective function value is in close proximity to its value in the three-dimensional solution. Please refer to Figure (3) for a visual representation of this process.

3 Three-dimensional simulation model

To achieve a model for three-dimensional simulation, the model must be examined and validated. Since no experimental data is available for the geometry of interest in this study, the validation and verification of the model have been carried out in two stages. First, simulations are performed on another geometry for which experimental data has been published in reference [2] (henceforth referred to as the "validation sample"), and the results are compared with the contents of the mentioned reference.

Subsequently, the geometry of interest in this project is also meshed, and the relevant checks for grid independence and wall-adjacent height (y+) are presented to ultimately obtain a suitable model for simulating the geometry.

3.1 Modeling and analysis of the validation sample

3.1.1 Modeling of the validation sample

An S-shaped inlet geometry for which experimental information is available has been used for numerical solution validation, this geometry was constructed by Wellborn at the NASA research center in 1992 and has undergone numerous experimental tests [2]. Since then, the results of these experiments have been accepted and used as a basis for validating numerical simulations on S-shaped inlet geometries. The geometry used by Wellborn is shown in Figure (3). This geometry is actually formed by the intersection of two circular arcs, whose derivation is described in Equations (6) to (8).

$$x = \begin{cases} Rsin\theta & 0 \le \theta \le \frac{\theta_{max}}{2} \\ 2Rsin\left(\frac{\theta_{max}}{2}\right) - Rsin(\theta_{max} - \theta) & \frac{\theta_{max}}{2} \le \theta \le \theta_{max} \end{cases} \quad (6)$$

$$y = \begin{cases} Rcos\theta - R & 0 \le \theta \le \frac{\theta_{max}}{2} \\ 2Rcos\left(\frac{\theta_{max}}{2}\right) - R(1 + cos(\theta_{max} - \theta)) & \frac{\theta_{max}}{2} \le \theta \le \theta_{max} \end{cases} \quad (7)$$

$$z = 0 \quad (8)$$

In the above equations, R=102.1 cm, and θ max=60°. In this geometry, the cross-sections are circular and perpendicular to the centerline. The inlet radius r1=10.21 cm, and the exit radius r2=12.57 cm. Therefore, the ratio of the exit area to the inlet area is A2/A1=1.52. The radius of the intermediate sections is determined as a function of the inlet radius, exit radius, and exterior angle, according to Equation (9) [2]. For a better understanding of the parameters and the calculation method for the intermediate section radii, refer to Figure (4). Figures (5) and (6) show the generated mesh on the solution domain.

$$\frac{r}{r_1} = 1 + 3\left(\frac{r_2}{r_1} - 1\right)\left(\frac{\theta}{\theta_{max}}\right)^2 - 2\left(\frac{r_2}{r_1} - 1\right)\left(\frac{\theta}{\theta_{max}}\right)^3 \quad (9)$$

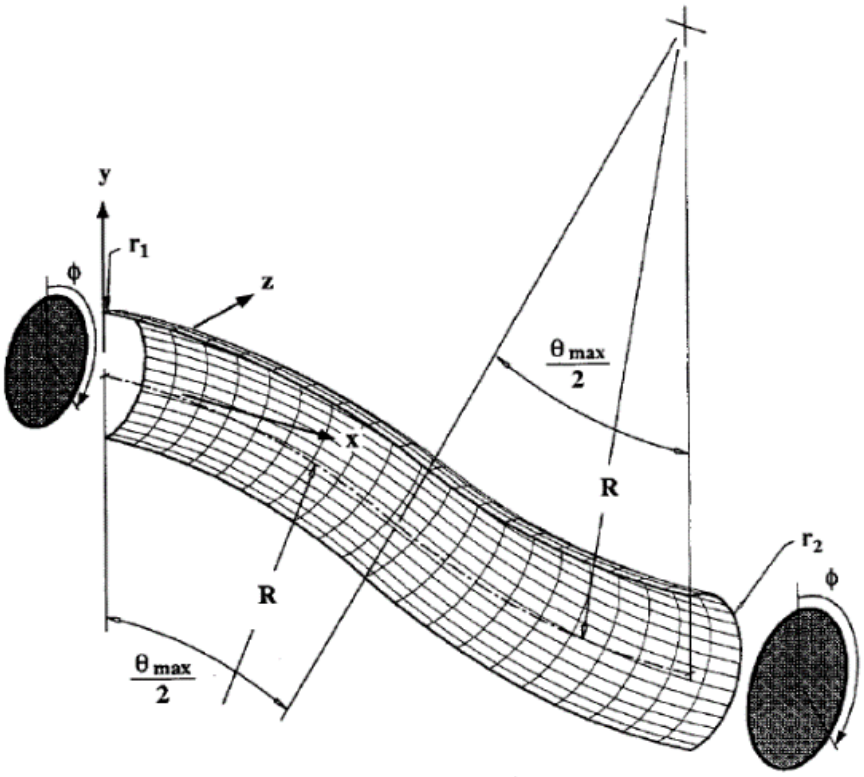

Figure 4 The geometry used by Wellborn [2]

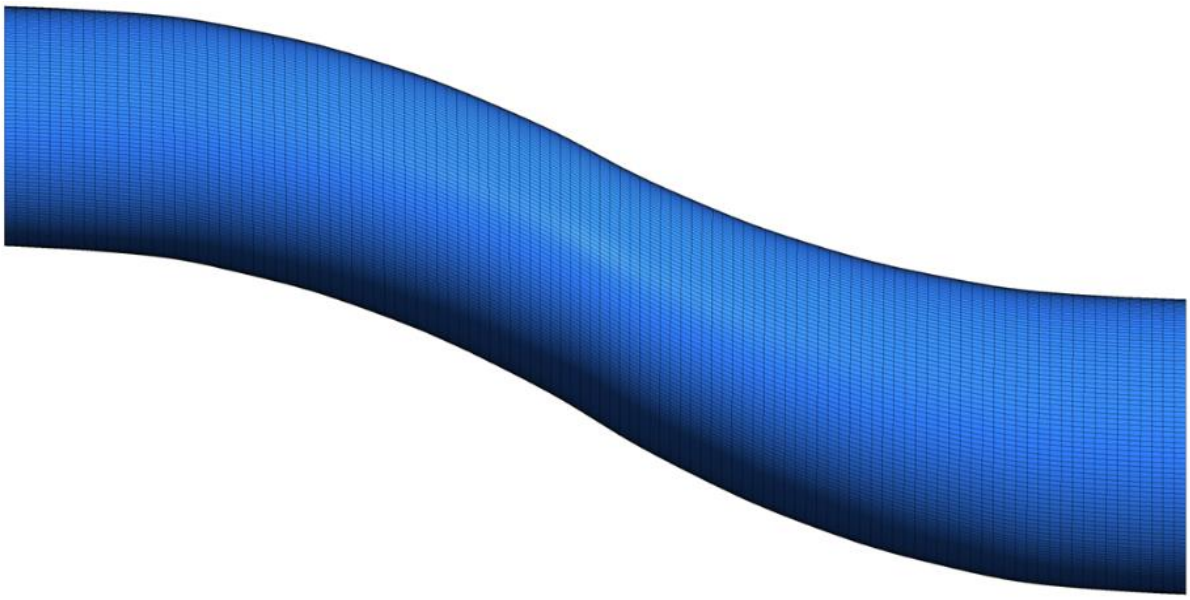

Figure 5 Side view of the generated mesh near the inlet duct wall (validation case)

Figure 6 Isometric view of the mesh near the duct wall (validation case)

3.1.2 Investigation of y+ in the validation case

For accurate boundary layer flow simulation, the wall-adjacent height (y+) is of great importance. The appropriate y+ value is a function of the turbulence model and the required boundary layer details. Since the SST turbulence model is used in the present simulation, the ideal y+ value is close to 1 [10]. To this end, the height of the first cell in the boundary layer must be adjusted such that y+ falls within an acceptable range. The variation of y+ along the 0 and 180-degree lines is shown in Figure (7). Additionally, the y+ contours are depicted in Figure (8). As can be seen, the y+ value in the validation geometry is close to 1 and within a completely suitable range.

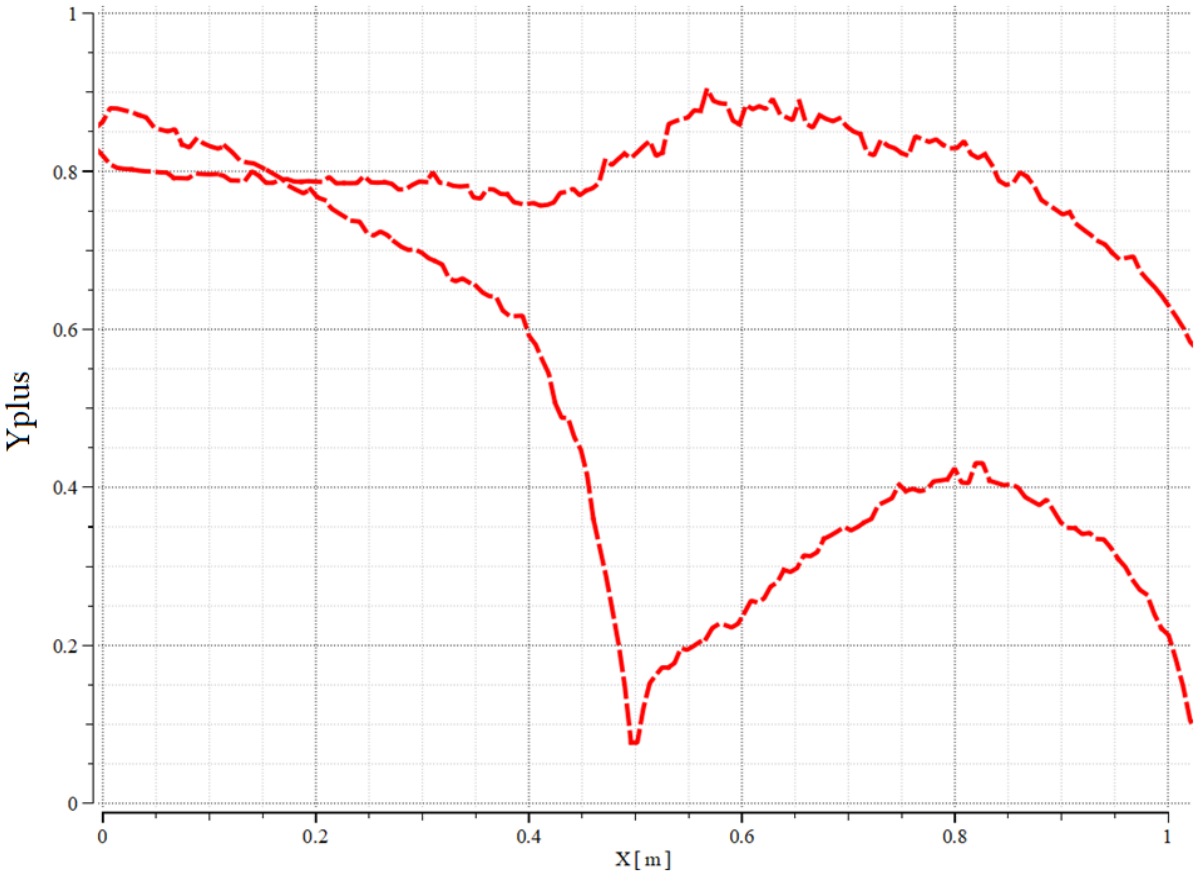

Figure 7 Variation of y+ along the φ=0 and φ=180 curves (validation case)

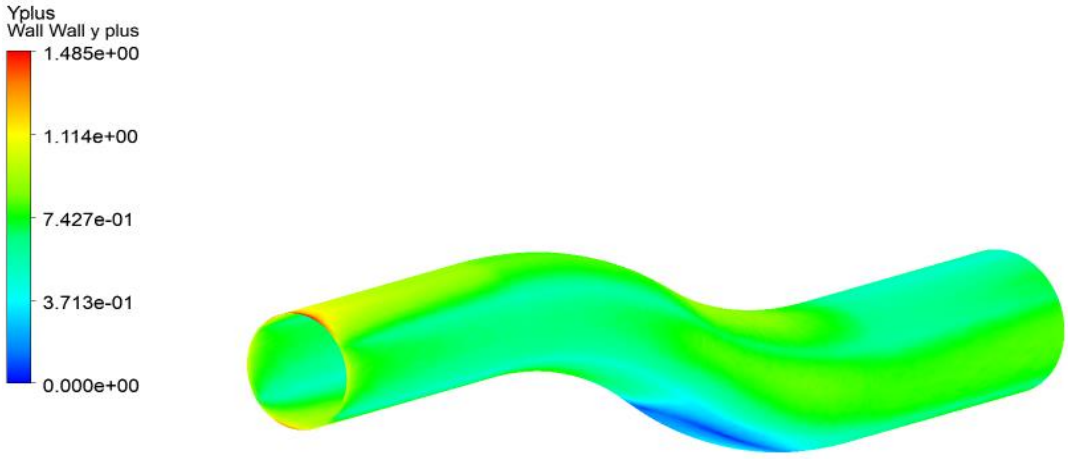

Figure 8 Contours of y+ variation on the wall (validation case)

3.1.3 Validation of results

The boundary conditions used for the validation geometry simulation are shown in Table (1). These boundary conditions are defined using the results of [4] to satisfy the experimental conditions reported in [2]. In [2], the inlet Mach number is 0.6, and the inlet Reynolds number based on the inlet plate diameter is 6.2 million.

To compare the simulation results with the experimental values, the total pressure recovery ratio contours at the exit plane (ratio of exit total pressure to the total pressure at the inlet plate center) are examined in Figure (9).

Additionally, the pressure coefficient distribution along the φ=10 and φ=170 lines, which are the experimental and numerical simulation results from [2], is presented in Figure (9). The comparison of the present simulation results with the experimental data is shown in Figure (10). In Figures (9) and (10), the horizontal axis is the arc length non-dimensionalized by the inlet diameter (s/d, where s is the arc length and d is the inlet diameter). Furthermore, the pressure coefficient is calculated using Equation (10).

$$Cp = \frac{P - P_{cl}}{P_{o,cl} - P_{cl}} \tag{10}$$

Where P is the static pressure, Pcl is the static pressure at the inlet center, and Po,cl is the total pressure at the inlet center. The difference between experimental and numerical results in Figures (9) and (11) is due to the non-deterministic definition of the flow separation region in a computational simulation, which often leads to errors. The rest of the experimental deviation can be attributed to flow separation throughout the air intake ducta since this takes place due to the high-pressure gradient and our highly curved validation geometry. On the whole, though, the numerical solution agrees with the experimental results.

Table 1 Boundary conditions for the validation case simulation

Boundary conditions	
Inlet total pressure	129240 Pa
Inlet total temperature	288 K
Outlet static pressure	114500 Pa

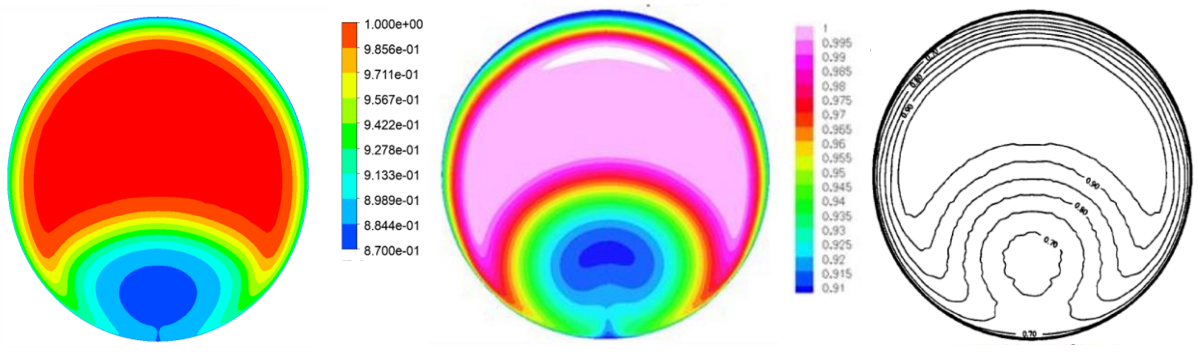

(**a**) (**b**) (**c**)

Figure 9 Comparison of exit total pressure recovery ratio contours (ratio of exit total pressure to inlet total pressure) from Wollburn's experiments [2] (**a**), numerical simulation of [3] (**b**), and the present simulation (**c**) (validation case)

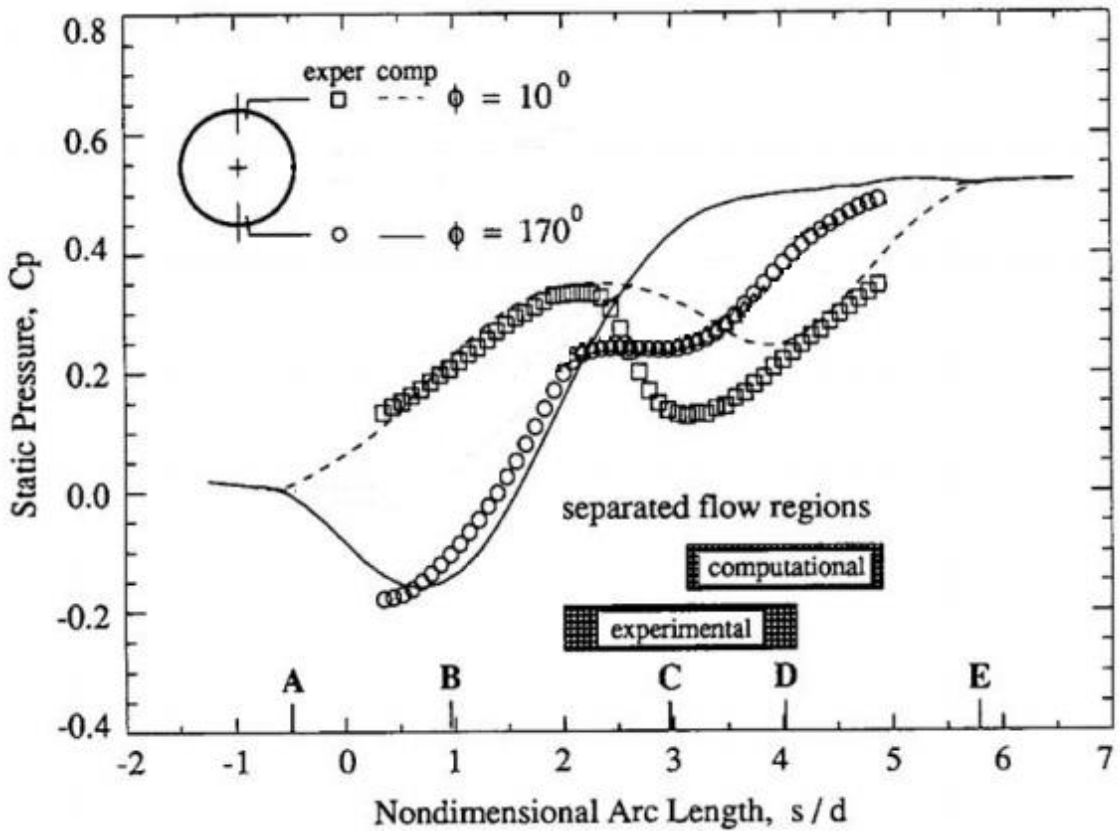

Figure 10 Comparison of pressure coefficient variation along φ=10 and φ=170 lines from Wollburn's experiments [2] and the simulation reported in the same reference (validation case)

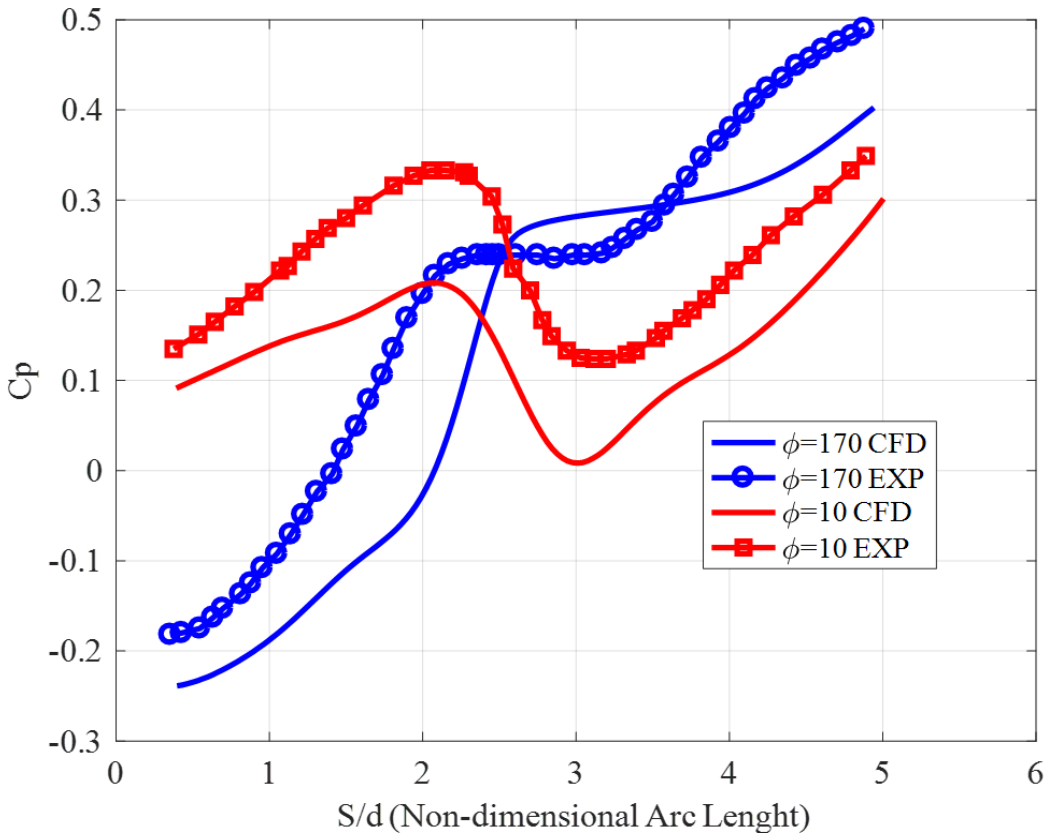

Figure 11 Comparison of pressure coefficient variation along φ=10 and φ=170 lines from Wollburn's experiments [2] and the present simulation (validation case) (In this figure, S and d are the arc length and inlet diameter, respectively)

3.2 Modeling the geometry of the present study

This section discusses the modeling of the geometry under investigation in the present study.

3.2.1 Computational domain mesh generation

In the present study, mesh generation is performed using the ICEM CFD software. Considering the capabilities of this environment, the computational domain is block-structured, and structured meshes are generated within each block.

Figure 12 Side view of the generated mesh near the inlet duct wall

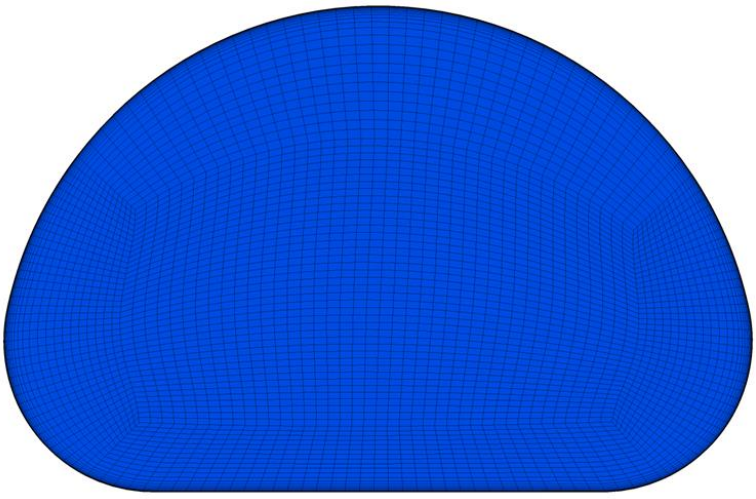

Figure 13 Mesh generated on the duct inlet plane

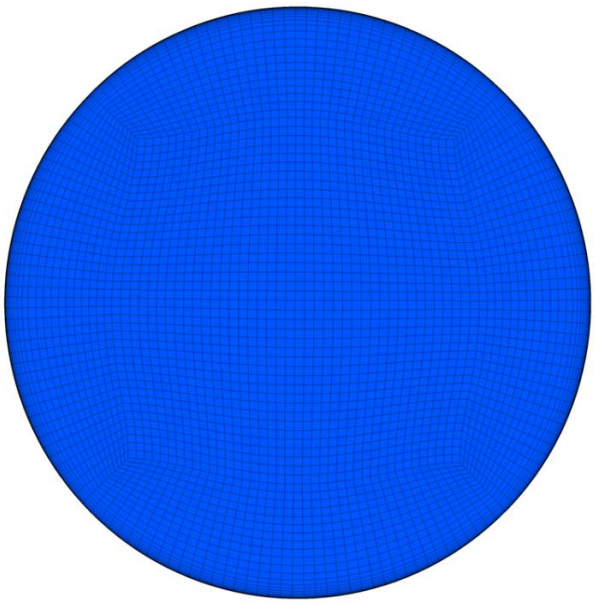

Figure14 Mesh generated on the duct outlet plane

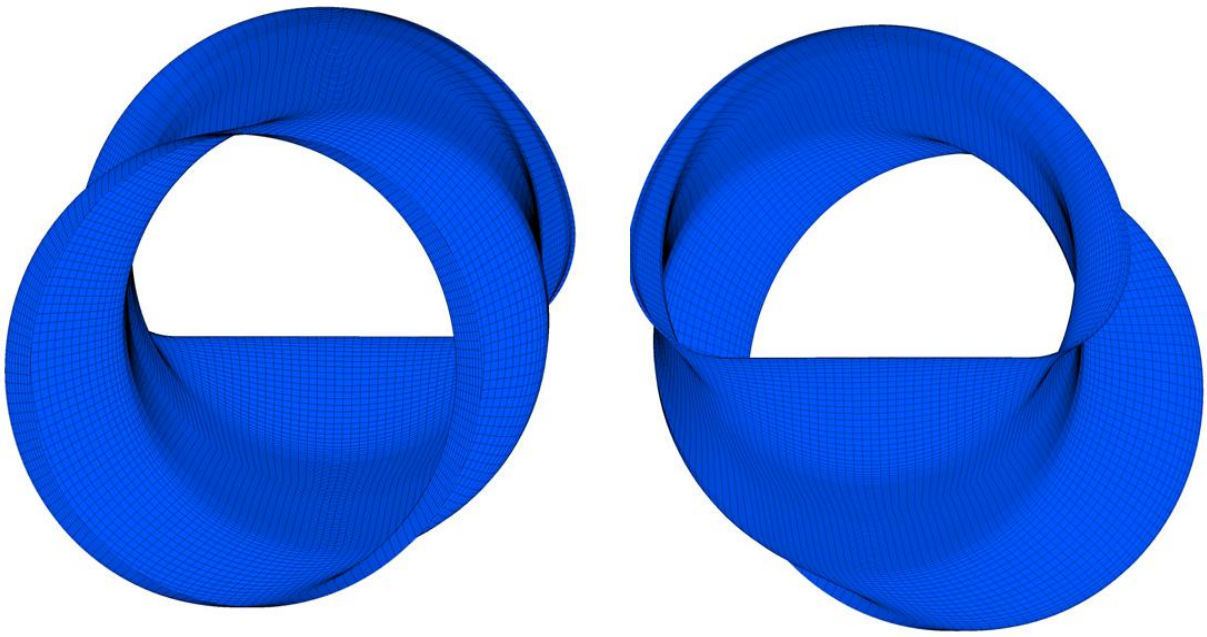

Figure 15 Mesh generated near the wall at the inlet (right figure) and outlet (left figure) cross-sections

Table 2 Specifications of the generated computational mesh

Generated computational mesh	
881,001	Number of nodes
864,000	Number of elements
3×10^{-6} m	Height of the first cell in the boundary layer

To accurately compute the parameters near the wall, a finer mesh is used, and the mesh becomes coarser towards the center. A factor that complicates the mesh generation process and consequently prolongs the solution process is that the air inlet duct under investigation is asymmetric due to layout considerations, and its cross-section varies along the air inlet duct length. Therefore, the entire domain (360 degrees) must be solved. Figures (12) to (15) illustrate the generated mesh on the computational domain. Additionally, the specifications of the generated computational mesh are presented in Table (2).

3.2.2 Solver settings

The solver employed in the present simulation is ANSYS CFX 2020R1. The settings adopted for the solution are as follows:

• Turbulence model: Considering the results published from research in the field of simulation and prediction of pressure drop at the aircraft inlet (such as references [4, 8-10]), the SST model has been utilized as the turbulence model.

• Boundary conditions: The applied boundary conditions are presented in Table (3). the inlet Mach number is 0.0 and the outlet Reynolds number based on the outlet plate diameter is 3.687 million. It should be noted that the inlet must be able to provide a mass flow rate of 24 kg/s, which will be checked after the solution is obtained using the static pressure outlet boundary condition.

Convergence Criterion: The convergence criterion is set to achieve a precision of 10-6 or a maximum of 200 iterations. After completion, the difference between the inlet and outlet mass flow rates is also checked to ensure it is less than 0.01% of the inlet mass flow rate.

Table 3 Boundary conditions for solving the inlet geometry under study in the present research

Value	Boundary conditions	Location
Total Pressure = 101.325 kPa	Inlet	Inlet
Total Temperature = 288 K	Inlet	Inlet
Static Pressure= 90.430kPa	Opening	Outlet
	Wall	Wall

3.2.3 Mesh independence study for the geometry under investigation in the present research

Four meshes with different sizes were generated and solved to ensure a sufficiently refined mesh. The results are presented as curves of Mach number, mass flow rate, and total outlet pressure versus the number of mesh points for the four meshes with different sizes in Figures (16), (17), and (18). As observed, the results become nearly constant when the number of elements reaches 864,000. The calculated values for different meshes are shown in Table (4).

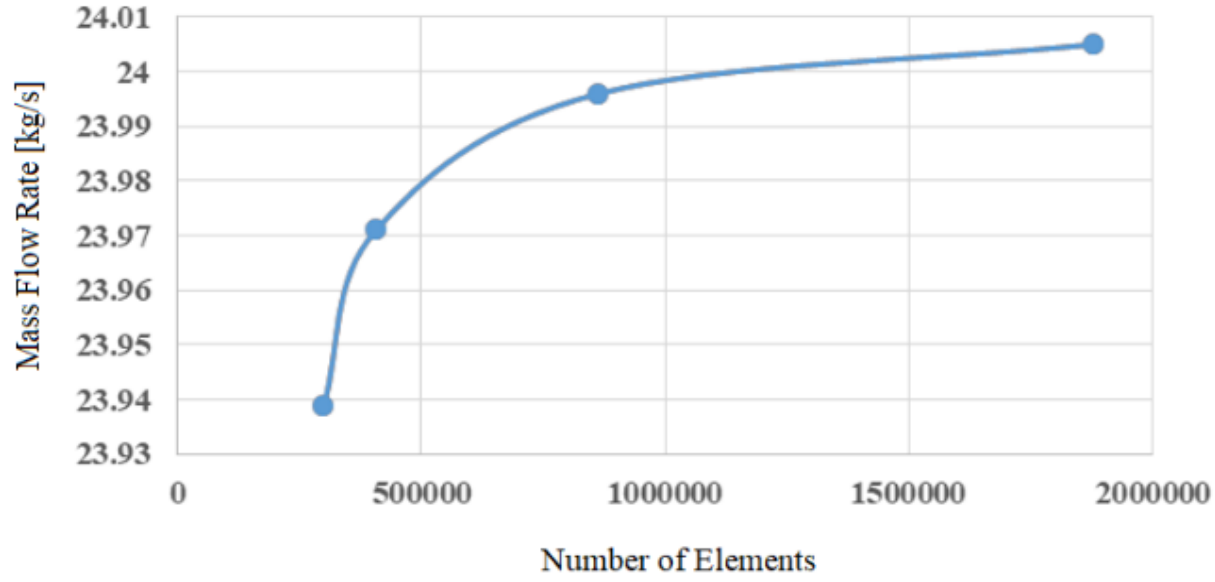

Figure 16 Mesh independence curve for mass flow rate

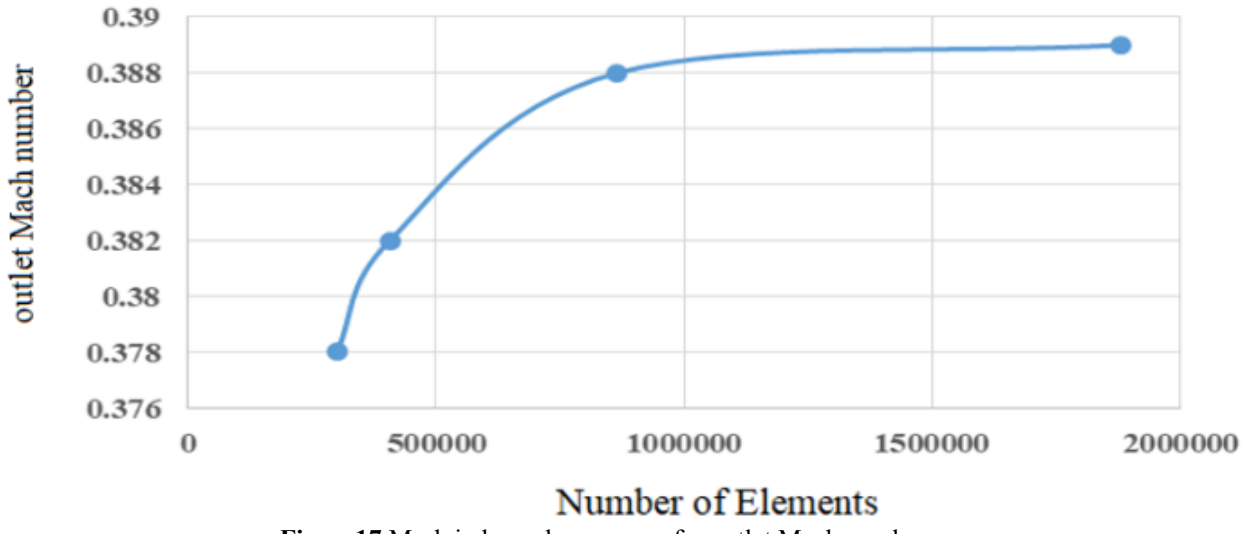

Figure17 Mesh independence curve for outlet Mach number

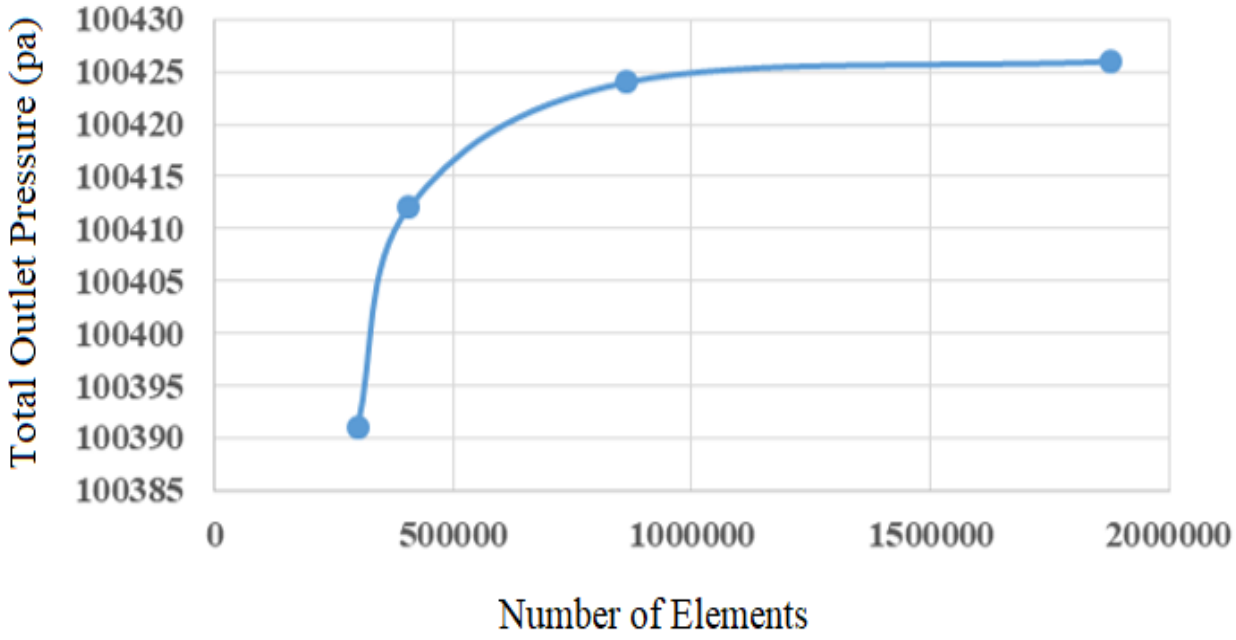

Figure 18 Mesh independence curve for total outlet pressure

Table 4 Results for meshes with different sizes

Total outlet pressure (pa) (Difference from the highest element count)	Outlet mach number (Difference from the highest element count)	Mass flow rate [kg/s] (Difference from the highest element count)	Number of elements
100391 (0.03%)	0.378 (2.83%)	23.939 (0.27%)	299520
100412 (0.014%)	0.382 (1.8%)	23.971 (0.14%)	406700
100424 (0.002%)	0.388 (0.26%)	23.996 (0.03 %)	864000
100426 (0)	0.389 (0)	24.005 (0)	1088000

Considering Figures (16) to (18) and the data presented in Table (3), it can be concluded that the mesh with 864,000 elements has acceptable accuracy, and the results become mesh-independent beyond this element count.

3.2.4 Evaluation of y+ for the geometry under investigation in the present research

Similar to the validation geometry, it is necessary to adjust the height of the first cell in the boundary layer so that y+ is close to 1, based on the studies previously conducted in research works [10].

The variations of y+ along the 0° and 180° lines are plotted in Figure (19). Additionally, the contour of y+ values is shown in Figure (20). These figures show that the y+ value is close to 1 and within an acceptable range.

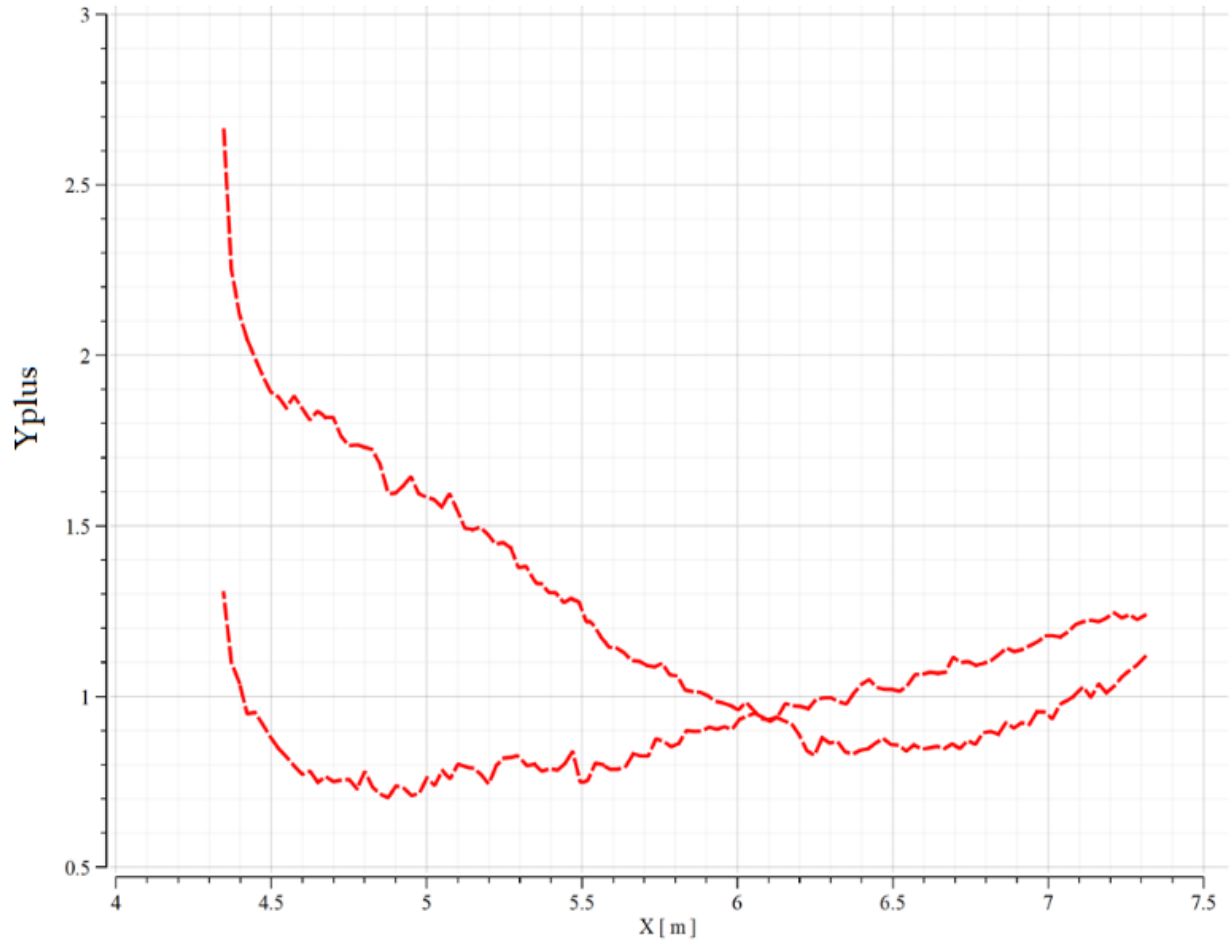

Figure 19 Variation of y+ along the φ=0 and φ=180 lines for the baseline geometry

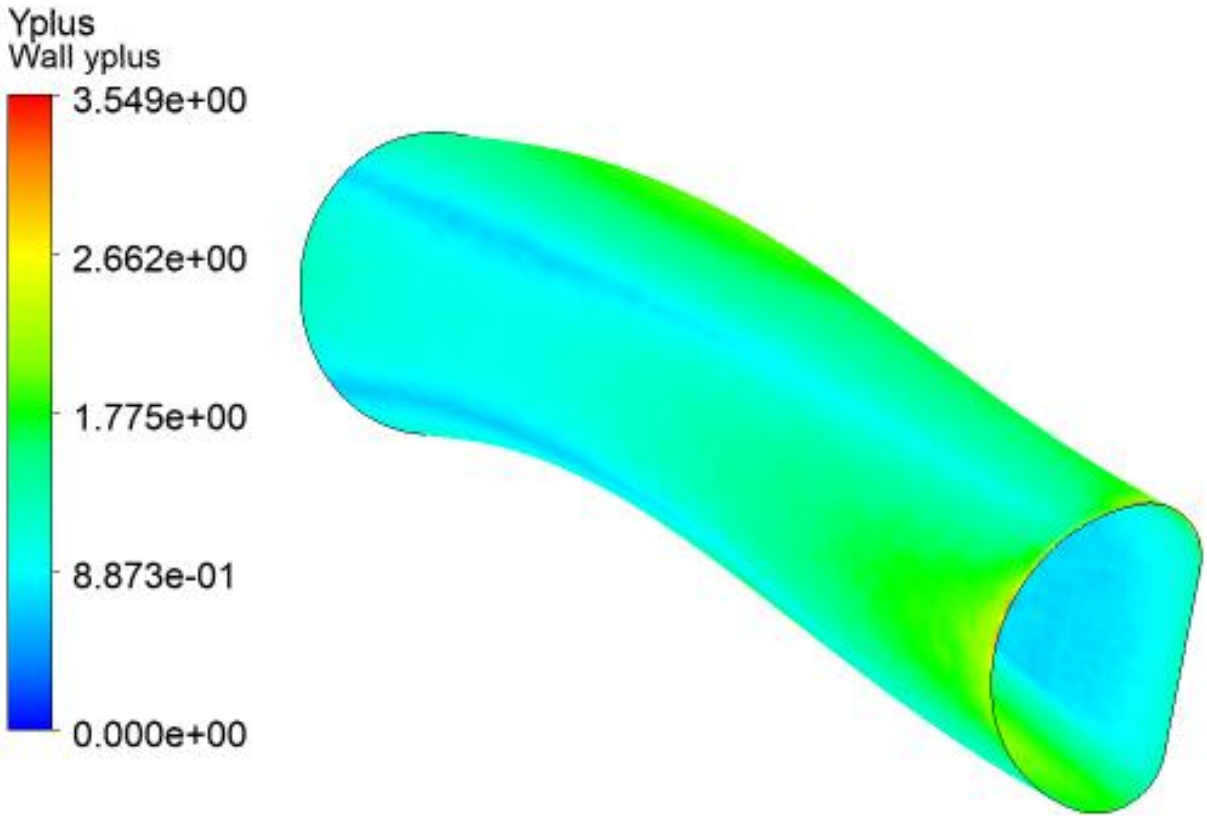

Figure 20 Contour of y+ on the wall of the baseline geometry

3.2.5 Results of solving the baseline geometry under investigation in the present research

Figure (21) shows the residual plots for mass and momentum as a function of the number of iterations.

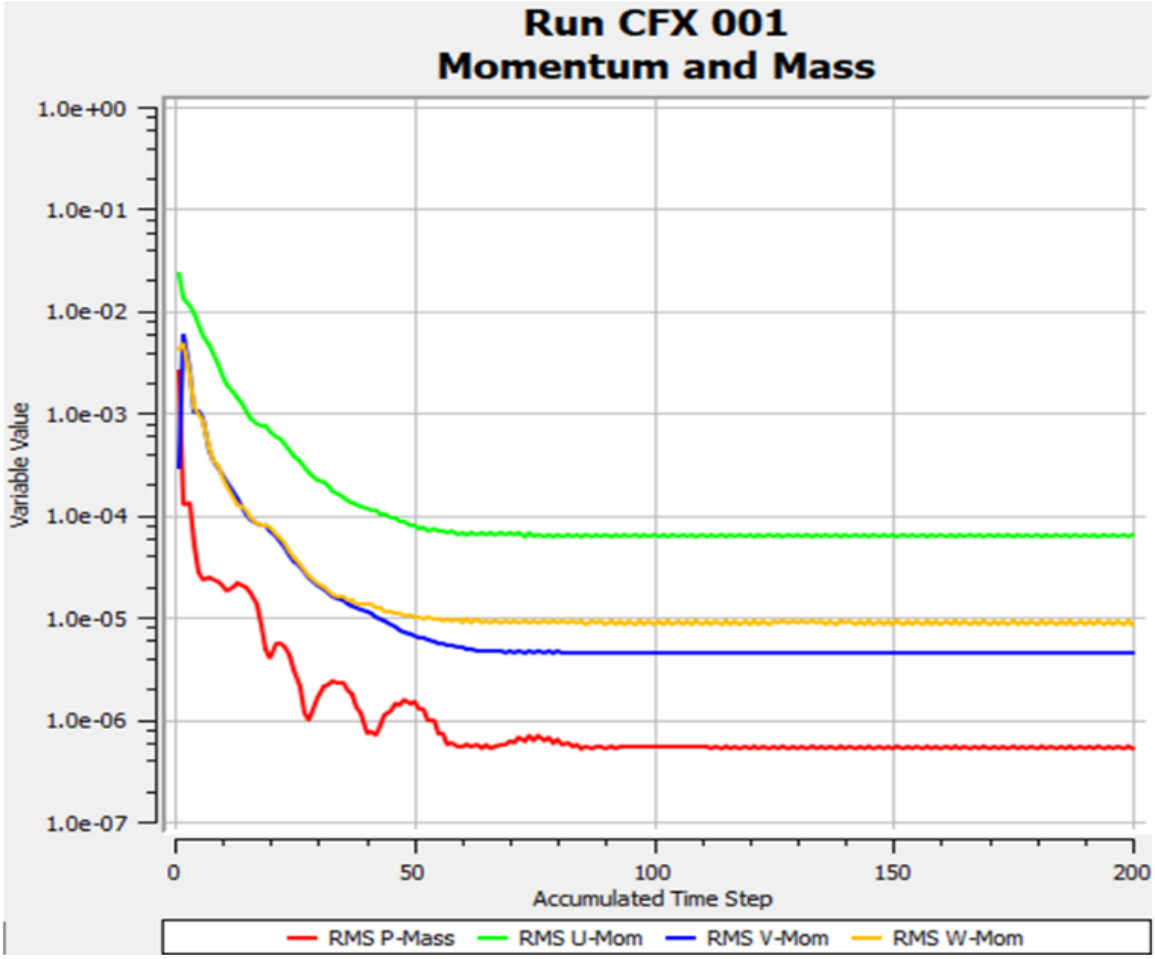

Figure 21 Residual plots for mass and momentum versus the number of iterations

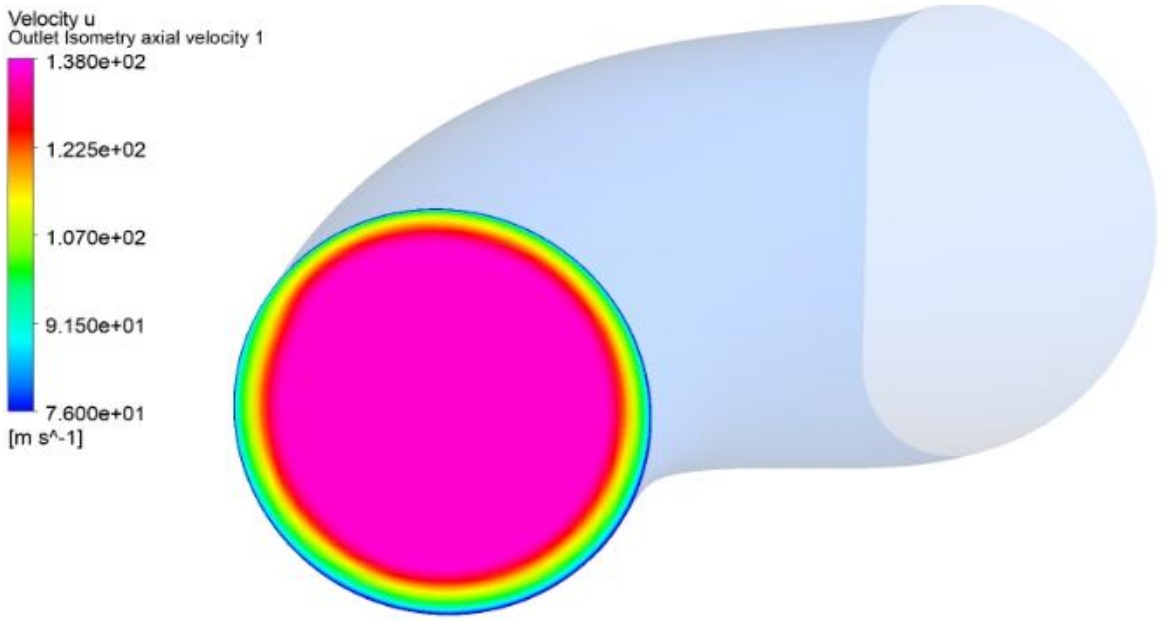

Figure 22 Axial velocity contour on the outlet plane of the baseline geometry at zero inlet Mach number

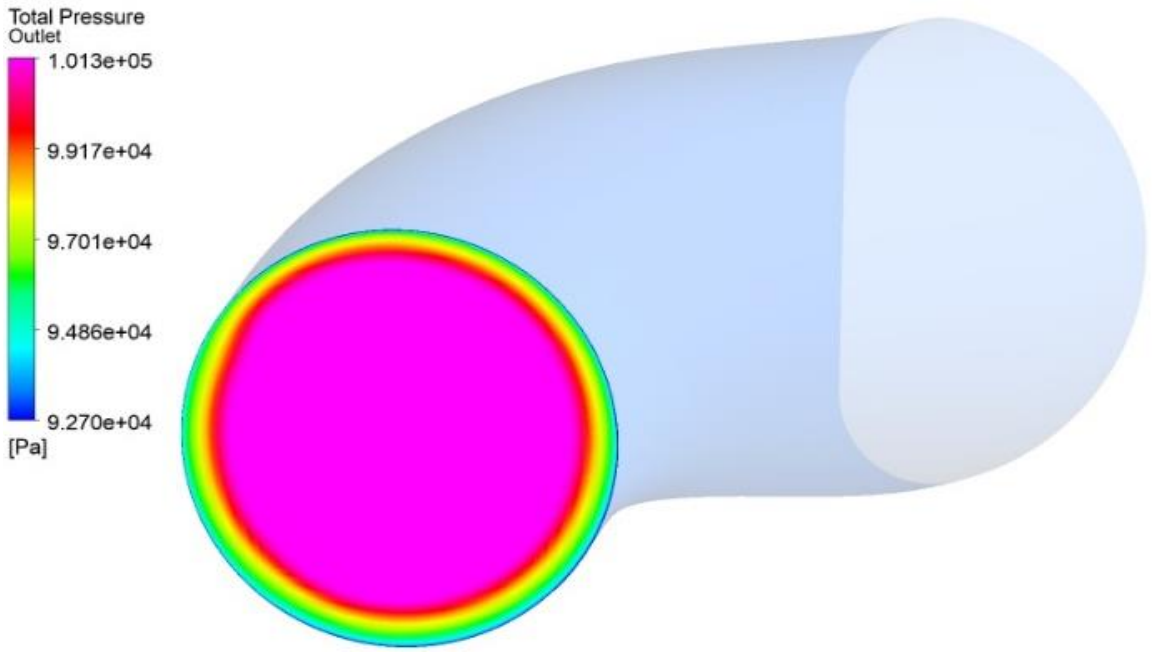

Figure 23 Total pressure contour on the outlet plane of the baseline geometry at zero inlet Mach number

Figure (22) displays the axial velocity contour on the outlet plane of the baseline geometry, and Figure (23) illustrates the total pressure contour on the outlet plane of the baseline geometry. As evident, there is an asymmetry in the distribution of total pressure and axial velocity at the inlet exit plane. This asymmetry arises from the curvature of the inlet duct wall, which leads to boundary layer growth and total pressure loss due to the wall curvature. In fact, reducing this asymmetry in the total pressure distribution is one of the objectives we aim to address during the optimization process. Another objective is to minimize the total pressure loss caused by the wall curvature.

3.2.6 Calculation of total pressure loss and flow distortion

Using Equations (2) and (3), the total pressure loss and distortion coefficient values for the baseline geometry at zero Mach number are calculated to be 0.009 and 0.032, respectively.

4 Optimization process

4.1 Generation of the initial database

4.1.1 Journal generation for meshing and flow simulation

As mentioned earlier in this report's introduction, this research aims to optimize the engine inlet geometry, which requires generating and evaluating the performance of many geometries through numerical simulations. Therefore, journal generation for meshing and flow simulation refers to creating a code (journal) capable of invoking various generated geometries, meshing them, and conducting numerical simulations. Since the initial geometries are ultimately rendered in 3D in Catia software, this stage necessitates the creation of three complementary and separate journals. These three journals are as follows:

First Journal: It invokes the geometry generated by Catia and converts it into ICEM geometry. This step is done in Ansys Workbench using Design Modeler. The task of this journal is to convert the geometry from .stp format to .tin format.

Second Journal: It generates the mesh on the geometry produced in the first step. This step is carried out in ICEM.

Third Journal: Using the mesh generated in the second journal, the flow is numerically solved, and the results are recorded. This step is carried out in CFX. These three journals are invoked sequentially in the MATLAB environment, thereby simulating the flow. Further details regarding the three journal processes for mesh generation and flow simulation are provided at the end of the report.

4.1.2 Geometry generation

This stage is divided into two parts. In the first part, a code must be written to generate the coordinates of acceptable random geometries. In the second part, a code must be written that can automatically create a 3D model of the generated geometry by invoking the results from the first part. This process is carried out as follows:

- Creating random geometries is accomplished through coding in MATLAB.
- Modeling the geometry using Catia software.
- Generating the ICEM geometry

The geometry model created in Catia must first be imported into the Design Modeler environment and saved in .tin format. This saved geometry can then be invoked in ICEM software for mesh generation.

- ICEM mesh generation

A journal is created for mesh generation on the ICEM geometry. MATLAB writes this journal, creates a mesh for the geometry created in the previous step, and checks if the mesh is valid.

- Numerical solution in ansys CFX

A journal was developed in Ansys CFX to solve the mesh generated in the previous step of this study. MATLAB invokes this journal to solve the mesh numerically.

4.2 Neural network training

One of the usual methods is to apply a neural network to define the relationship between the dependent and independent variables in systems with a high degree of complexity. The neural network is a method for determining the nonlinear and intricate relationship between independent and dependent variables without any consideration of the physical model of the problem.

Therefore, there must be a finite number of independent variables along with their dependent variables. The accumulation of these independent variables and their dependent variables is known as a database.

The way it works is that the network is trained to understand how the independent variables in the problem, which could be vectors or matrices, influence specific dependent variables; these could be scalars, vectors, or matrices. The more independent and dependent variables within a problem, the simpler it becomes for the neural network to learn.

4.2.1 Structure of the neural network

As mentioned earlier, in this project, the independent variables that define the random geometry of the inlet consist of 7 values. Therefore, we are dealing with a database with a 7-element input vector representing the input samples. Additionally, in each sample, there are two dependent variables (flow pressure loss and flow distortion). A separate neural network is trained for each of these two dependent variables to reduce the complexity of the neural network training and enhance its learning accuracy. The neural network training structure can be summarized as shown in Figure (24).

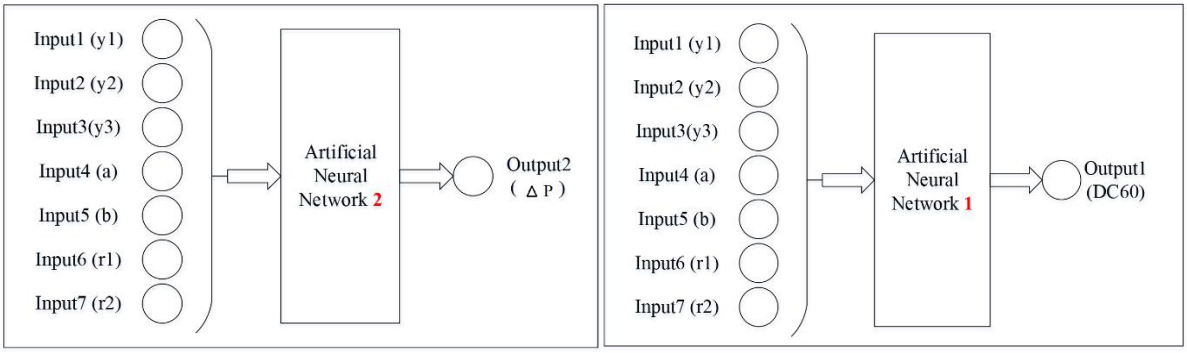

Figure 24 Overview of neural network training (number of networks, inputs and outputs)

4.2.2 Neural network training settings

- To start the training process, 70% of the data is allocated for training, 15% for testing, and 15% for validation.
- The learning inertia coefficient is set to 0.9.
- All other settings remain at their default values in MATLAB.
- Configuring the Genetic Algorithm Settings

Training Function:
Understanding which algorithm works faster for a specific problem is complex. This issue depends on various factors, among which we can mention the complexity of the situation, the number of test data, the number of network weights, the desired error, and whether the network is used for pattern recognition or function approximation. The results of the current study showed that the Trainer function, as a neural network training function, performs better for both variables under study in the research and has a faster learning speed and higher accuracy. Since neural network training also depends on the initial guess of the weight matrix this weight is randomly selected for each training series. In the current study, 100 different trainings were performed for each tested configuration and the network with the lowest error was saved as the desired network. This process is then repeated until we ultimately achieve the minimum error. If we do not reach the desired error for a configuration, we change the configuration and repeat the above process. In this study, after performing the above process to calculate the pressure loss to the neural network of Cascade-forward networks type with the layout [14, 3], the network configuration is shown in Figure (25).
The final stopping criterion for the training process is set such that the maximum error calculated for 55 input data series in the database is less than 1 percent. In the trained neural network for pressure loss calculation, the maximum error is 0.3128 percent (i.e., less than half a percent). The comparison between the results from the three-dimensional flow solution and the neural network output for total pressure loss calculation is shown in Figure (26).

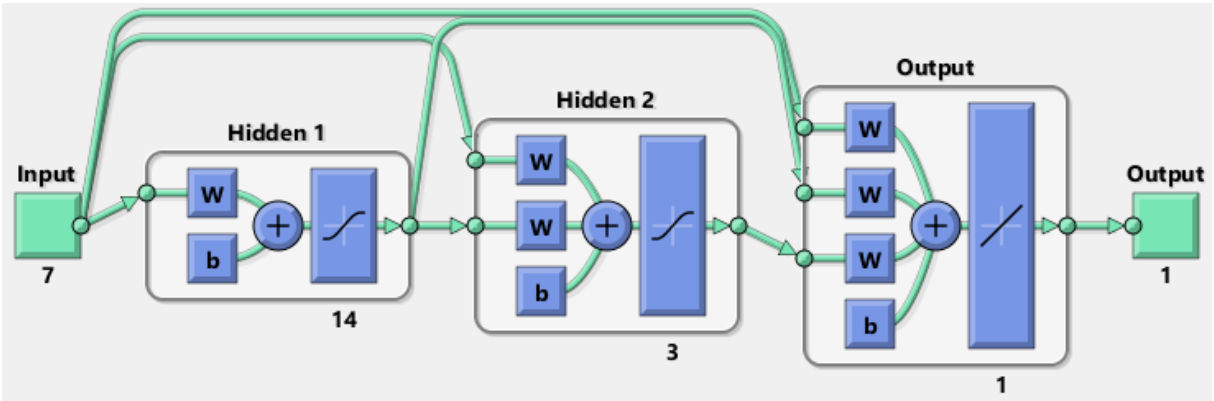

Figure 25 Configuration of trained neural network to calculate total pressure loss

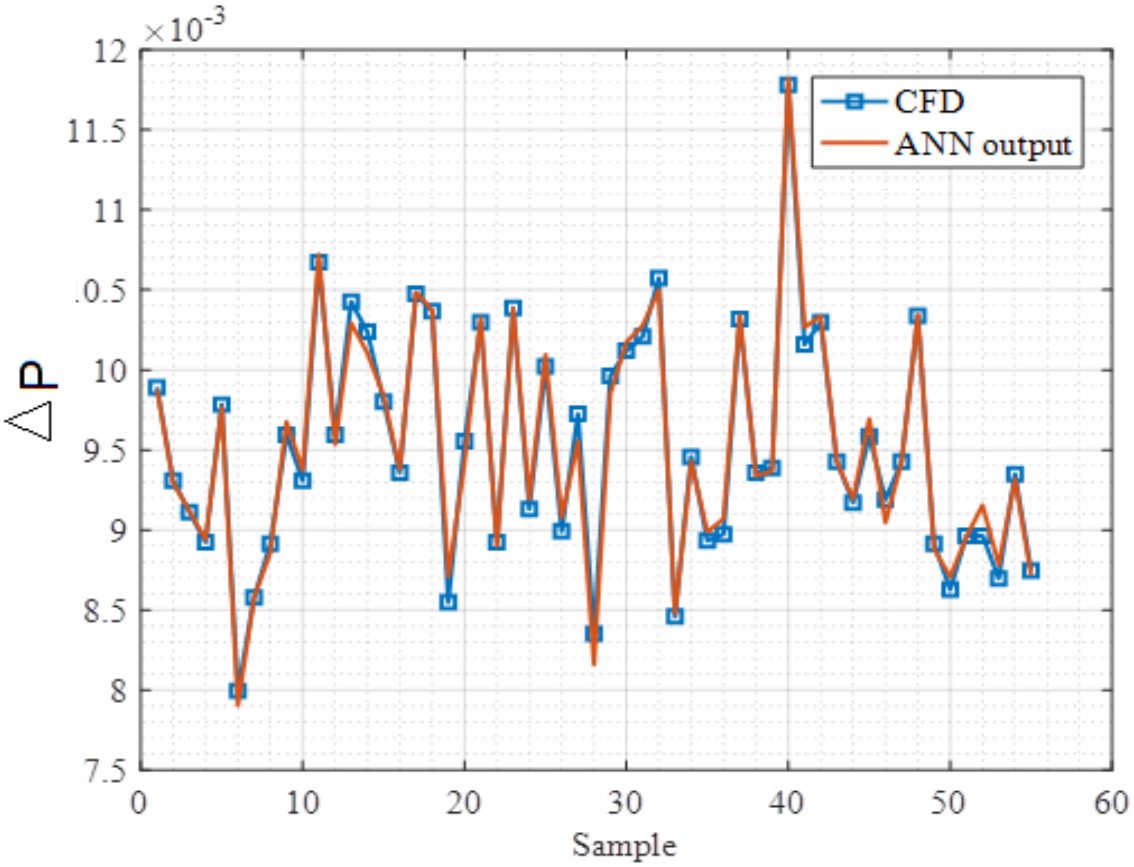

Figure 26 Comparison of results from the three-dimensional flow solution and the neural network output for total pressure loss calculation

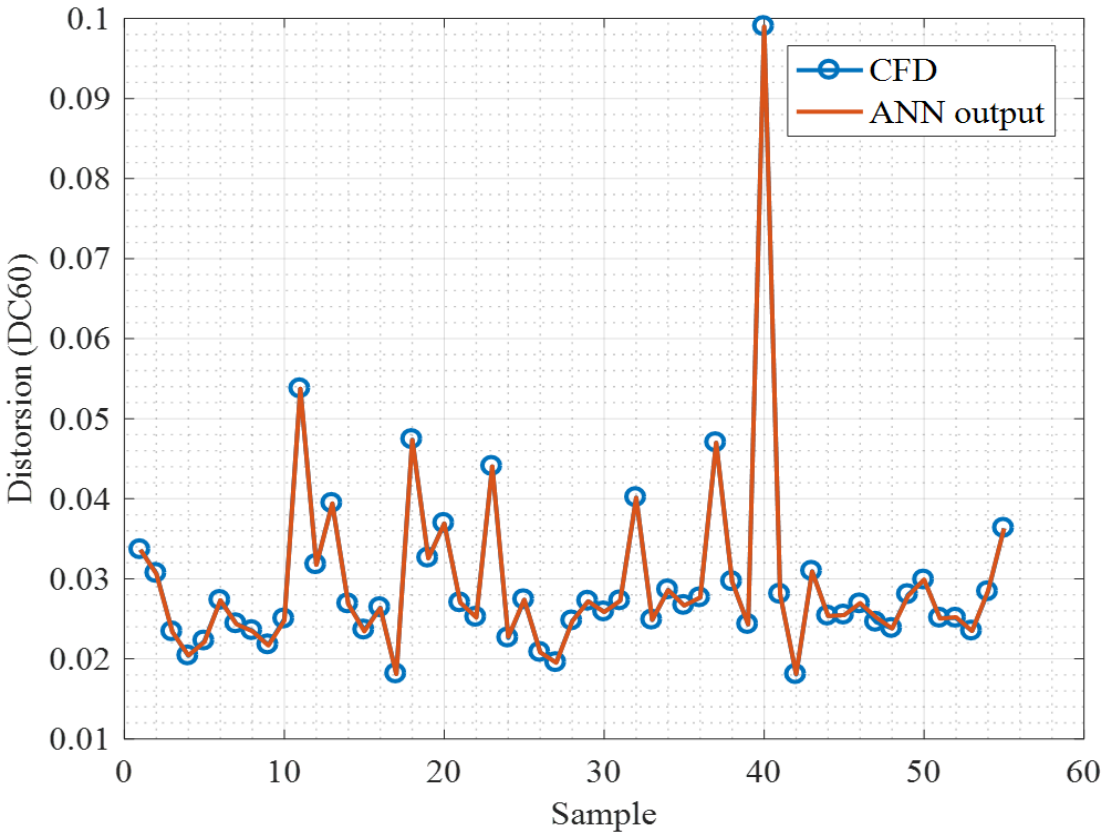

Figure 27 Comparison of results from the three-dimensional flow solution and the neural network output for outlet flow distortion calculation

In the trained neural network for distortion calculation, the maximum error is 0.3964 percent (i.e., less than one percent). The comparison between the results from the three-dimensional flow solution and the neural network output for outlet
flow distortion calculation is shown in Figure (27). Additionally, as observed in Figures (26) and (27), the neural network output shows excellent agreement with the three-dimensional solution results (database data).

4.3 Optimization by genetic algorithm

MATLAB's genetic algorithm function was used for the optimization process. To conduct any optimization process, the following steps must be followed:

- Defining the objective function
- Defining constraints to limit the search space
- Configuring the genetic algorithm settings

4.3.1 Defining the objective function

The objective function was discussed in Equation (5). An entirely separate neural network has been trained to compute each of the two components of the objective function (pressure loss and flow distortion). Thus, to evaluate the objective function using the input geometry, the values for flow distortion and pressure drop are first computed by calling the respective neural networks. Then the objective function is obtained by summing the two.
When adding the objective function to the genetic algorithm, it is necessary to create an m-file defining the objective function and call it in the genetic algorithm command.

4.3.2 Determination of design constraints (geometric, logical, and installation considerations)

The design constraints are as follows:
1-Considerations for the inlet duct installation on the aircraft.
Regarding the installation considerations for the inlet duct, the following requirements must be met:
• The inlet duct shape and coordinates from the inlet leading edge to the initial throat are fixed.
• For a length of 150 mm from the duct exit, it is a straight cylindrical section.
These requirements ensure that the inlet duct's initial and final sections remain fixed, and the optimization process is performed for the intermediate sections of the inlet duct. (See the figure below)
2-To satisfy the inlet diffusion process, the cross-sectional area must continuously increase along the inlet duct length (the inlet duct cross-sectional area must strictly increase in the longitudinal direction).
3-Given that the y-component of the engine center is less than the y-component of the initial inlet center, to avoid flow separation, the y-component of the maximum y-curve of the inlet duct cross-sections from the inlet to the engine must strictly decrease.
4-To avoid generating an undulating geometry, the concavity of the maximum y-curve of the inlet duct cross-sections from the inlet to the engine must change at most once; hence, this curve can have at most one inflection point.
5- Given that the maximum z-component of the engine cross-section is greater than the maximum z-component of the initial inlet cross-section, to avoid flow separation, the z-component of the maximum z-curve of the inlet duct cross-sections from the inlet to the engine must strictly increase.

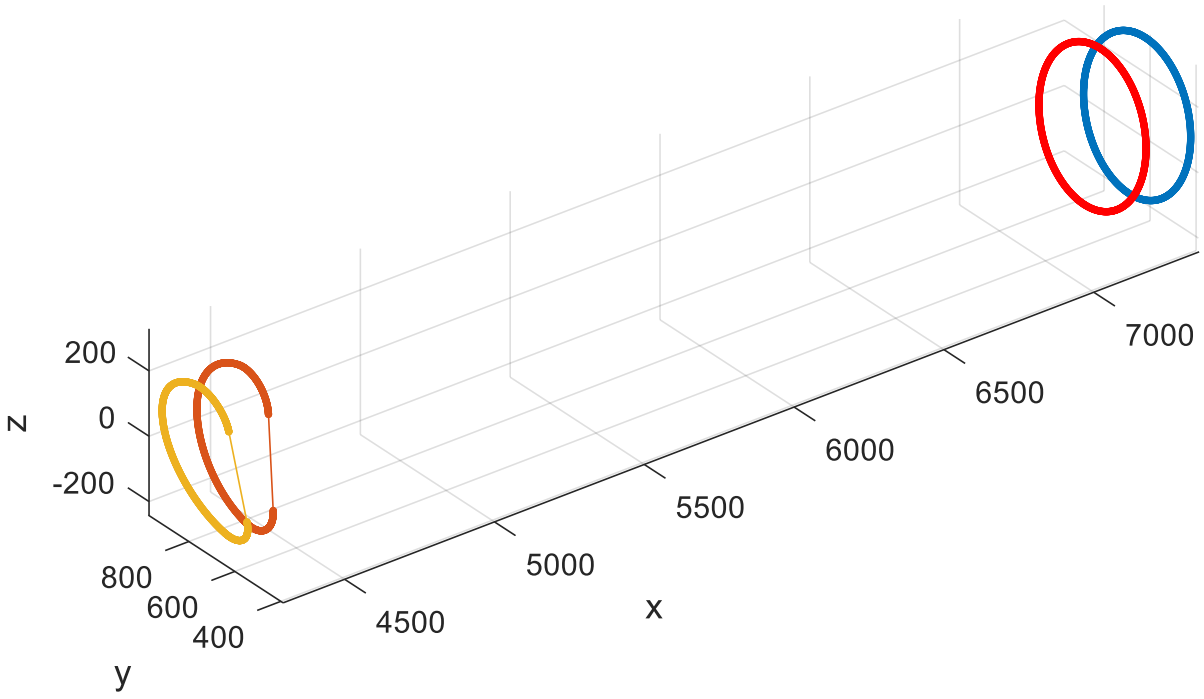

Figure 27 Constraints arising from the inlet duct installation considerations (fixing the initial and final sections of the inlet duct)

6- To avoid generating an undulating geometry, the concavity of the maximum z-curve of the inlet duct cross-sections from the inlet to the engine must change at most once; hence, this curve can have at most one inflection point.

The penalty function determines the maximum allowed deviation from the constraint during the optimization process, which is set to 10^{-8}.

4.3.3 Configuring the genetic algorithm

- *Population size:*

This represents the number of geometries produced and evaluated in each generation of the Genetic Algorithm process. A generation refers to a cycle of new offspring from the members of one generation, resulting in a new population. After each generation is produced, the objective function is evaluated for each generation member, and the members with better objective function values are selected to produce the next generation. In this study, the population size is set to 100.

- *Max generations:*

This parameter defines the total number of generations to be produced for optimization. If the stopping conditions are not met, the optimization process will stop after reaching the specified number of generations. In this study, 500 generations have been set for the optimization process.

- *Constraint tolerance:*

This parameter determines the maximum allowable deviation from the constraints during the optimization process, which has been set to 1e-8 in this study.

- *Initial Population matrix:*

If it is known beforehand (for example, based on the database) that specific geometries yield better results, they can be introduced to the Genetic Algorithm. This helps accelerate the optimization process.

The **remaining settings** of the Genetic Algorithm are kept at their default values in MATLAB.

5 Results and discussion

5.1 Optimization results

The values of the geometric variables required for modeling the inlet duct, along with the total pressure loss and outlet flow distortion values, are presented in Table (5). Additionally, the three-dimensional model of the computed optimized geometry is shown in Figure (29).
According to the information in Table (6), a geometry with a flow distortion value of 0.00754 and a total pressure loss value of 0.00752 was obtained at the end of the optimization stage. Compared to the baseline geometry values (0.0315 for flow distortion and 0.0089 for total pressure loss), this represents a more than 76% reduction in flow distortion and a more than 15% reduction in total pressure loss. However, these values are based on the neural network evaluation and must be validated further.

Table 5 Parameters obtained from optimization using the genetic algorithm (cross-sectional center coordinates, minor and major ellipse radii, circle radii, pressure loss, and flow distortion)

Flow distortion	Total pressure loss	r_2(mm)	r_1(mm)	b(mm)	a(mm)	y_3(mm)	y_2(mm)	y_1(mm)
0.00754	0.00752	226.7339	226.7337	244.5744	208.7236	672.703	724.9315	762.5187

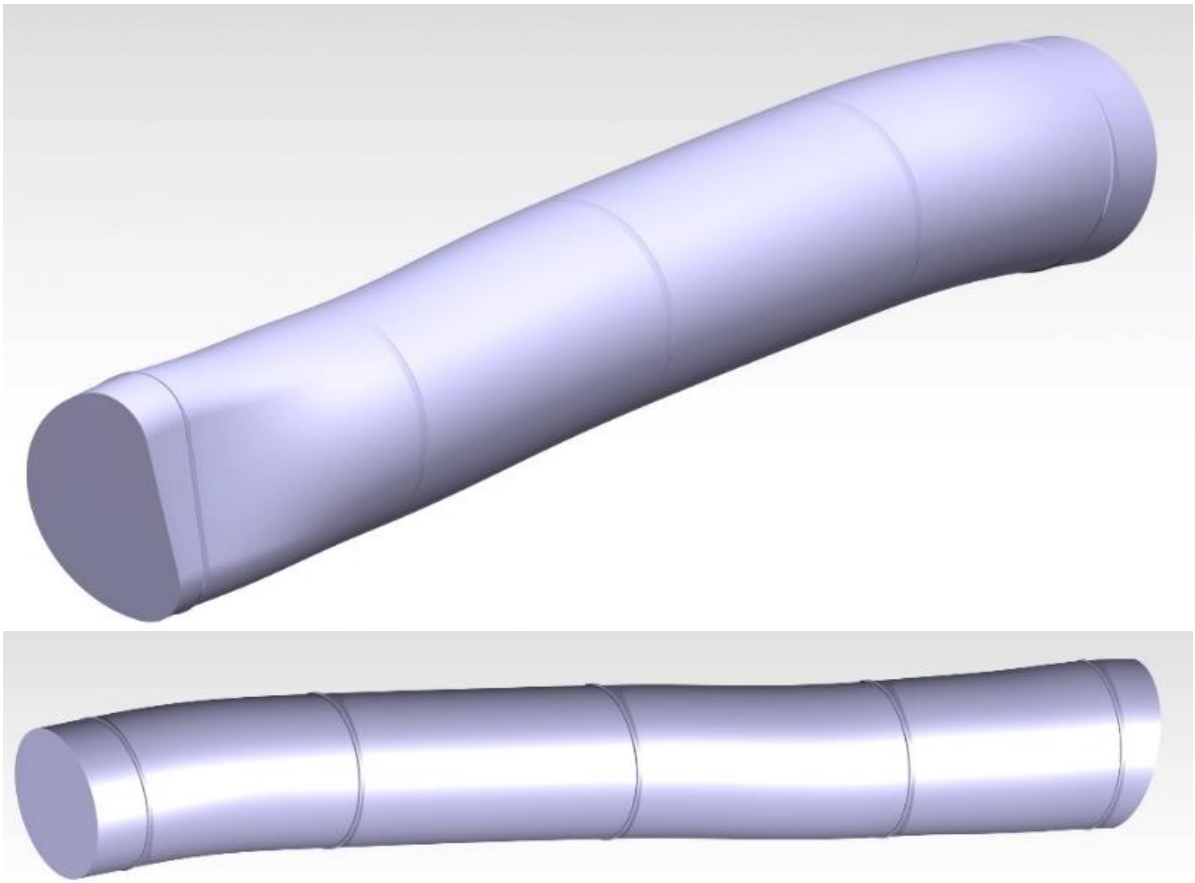

Figure 29 Three-dimensional model of the optimized geometry

5.2 Validation of optimization results

The genetic algorithm calls an objective function that is the output of two neural networks. These networks were trained on a database of 55 random geometry solutions. However, it is possible that the resulting geometry from the genetic algorithm may fall outside of the training data space, which could lead to objective function values that are not entirely accurate. After optimization, it is recommended that the resulting geometry be evaluated using a three-dimensional solution. This evaluation can then be compared with the neural network results for flow distortion and total pressure loss values. The resulting geometry will be accepted if the results are deemed sufficiently similar. In the event that the results are not similar enough, the geometry obtained from optimization, along with the calculated values for flow distortion and total pressure loss, will be added to the database. The process of training the neural networks and subsequently optimizing with the genetic algorithm will then be repeated. Please refer to Figure (30) for a visual representation of the flowchart for validating the inlet duct optimization. The values of pressure loss, flow distortion, and their sum (the objective function) are plotted in Figures (31) to (33), respectively.

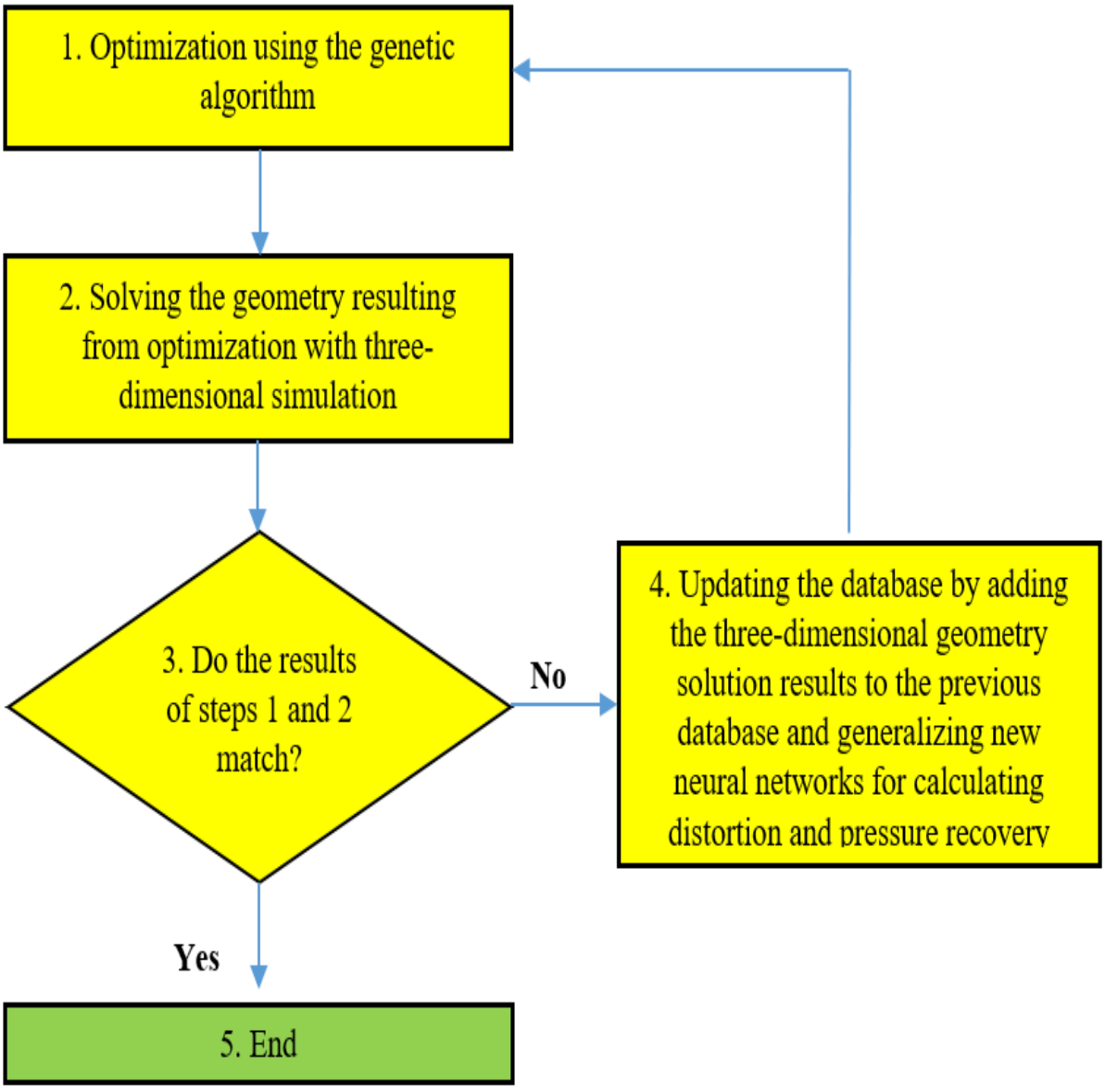

Figure 30 Flowchart for validating the inlet duct optimization

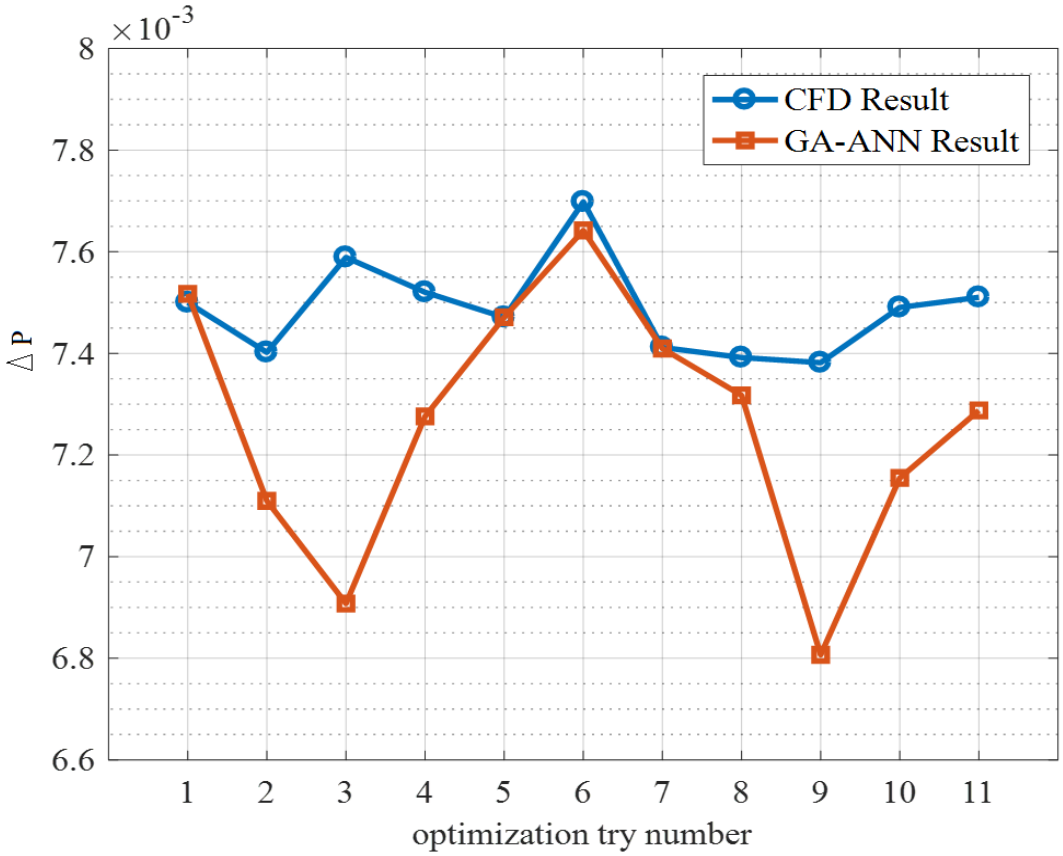

Figure 31 Comparison between the results of the genetic algorithm based on the neural network and its evaluation with the three-dimensional solution for total pressure loss

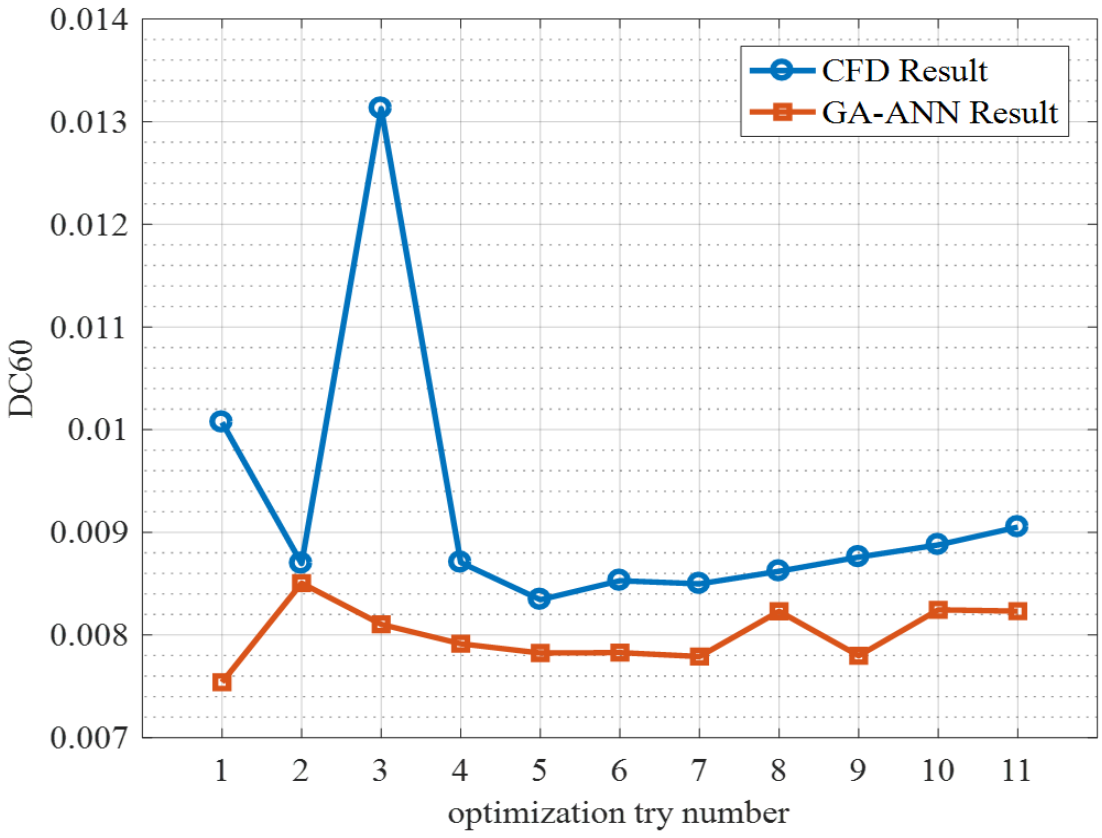

Figure 32 Comparison between the results of the genetic algorithm based on the neural network and its evaluation with the three-dimensional solution for flow distortion

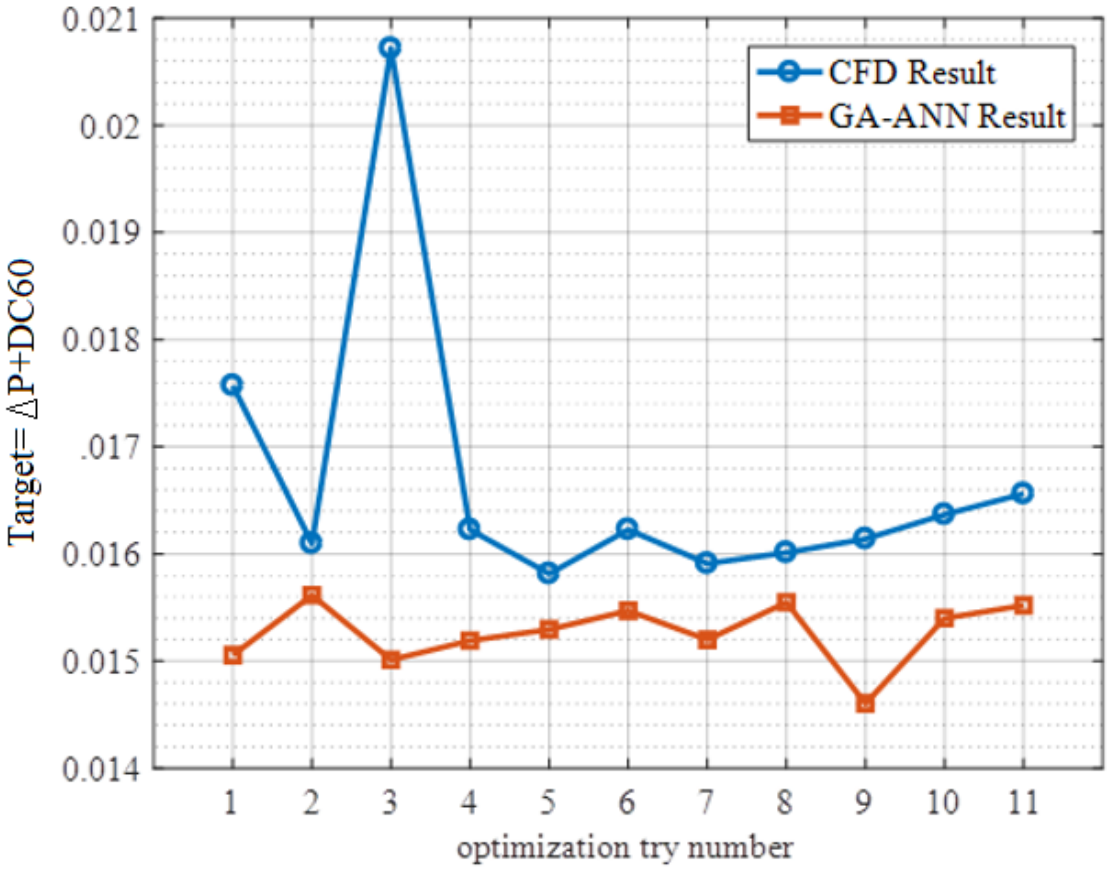

Figure 33 Comparison between the results of the genetic algorithm based on the neural network and its evaluation with the three-dimensional solution for the objective function

5.3 Comparison of baseline and optimized geometries

The comparison of flow distortion, total pressure loss, and objective function values for the baseline and optimized geometries is shown in Table (6). As observed, the performed optimization results in an improvement of more than 60% in the objective function. Additionally, the comparison between total pressure and velocity contours for the baseline and optimized geometries is shown in Figures (34), (35), (36) and (37). The increase in the average total pressure and the improvement in its distribution at the outlet plane can be clearly observed in figure (34). Furthermore, the improvement in the uniformity of the axial velocity at the outlet plane is seen in Figure (35).

In Figure (36) a comparison of the absolute pressure contour inside the duct in the xy plane for two baseline geometry and optimized geometry states is provided. In the optimized geometry due to the curvature of the duct geometry, the pressure gradient increases along the duct in a more uniform distribution than the baseline geometry state. This results in a reduction in the total pressure loss at the end of the duct and an increase in flow efficiency and uniformity.

Table 6 Comparison of flow distortion, total pressure loss, and objective function values for the baseline and optimized geometries

	Baseline Geometry	Optimized Geometry	Absolute Improvement	Relative Improvement (%)
ΔP	0.0089	0.0075	0.0014	16%
DC60	0.0315	0.0078	0.0237	74%
Target	0.0404	0.0153	0.0251	61%

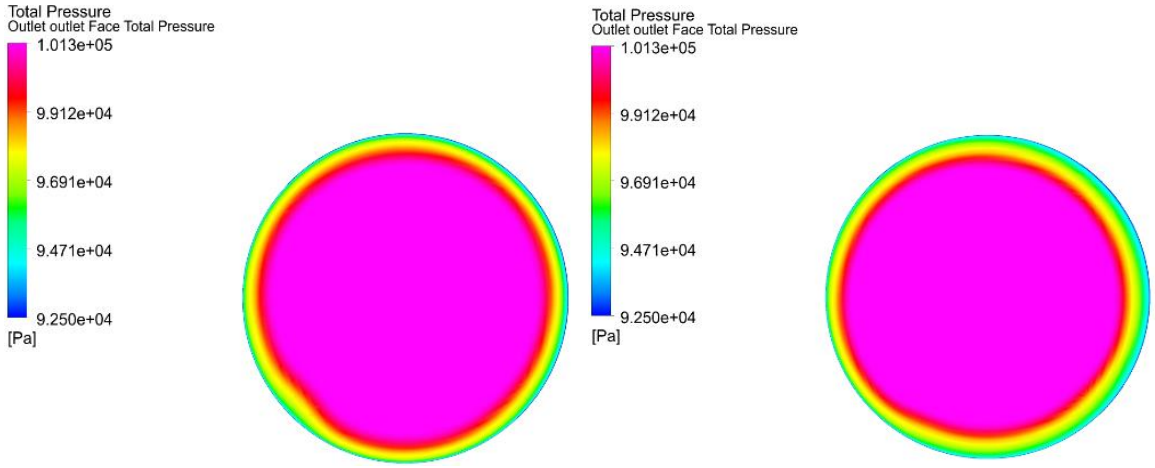

(**a**) (**b**)

Figure 34 Comparison of outlet total pressure contours for (**a**) the baseline geometry and (**b**) the optimized geometry

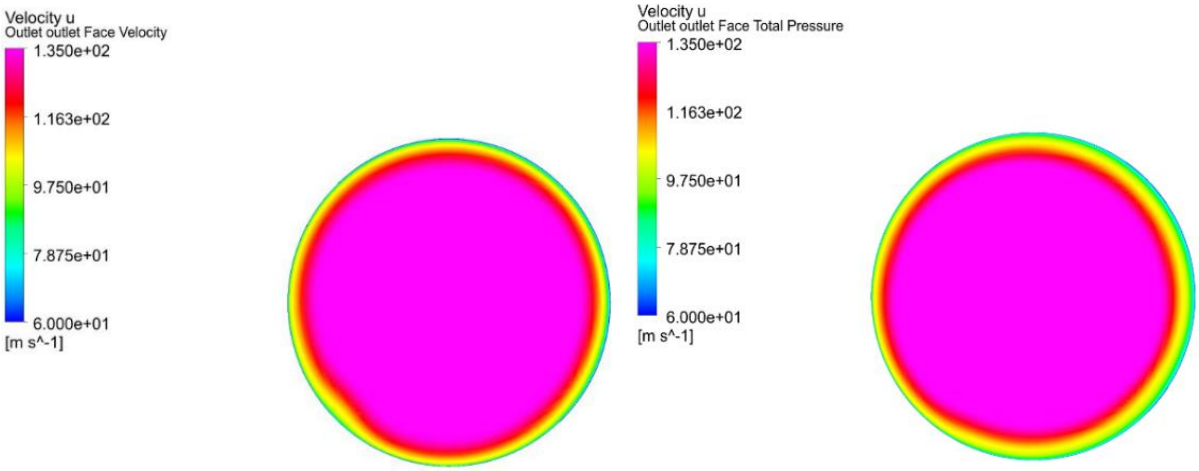

(**a**) (**b**)

Figure 35 Comparison of outlet axial velocity contours, (**a**) the baseline geometry and (**b**) the optimized geometry

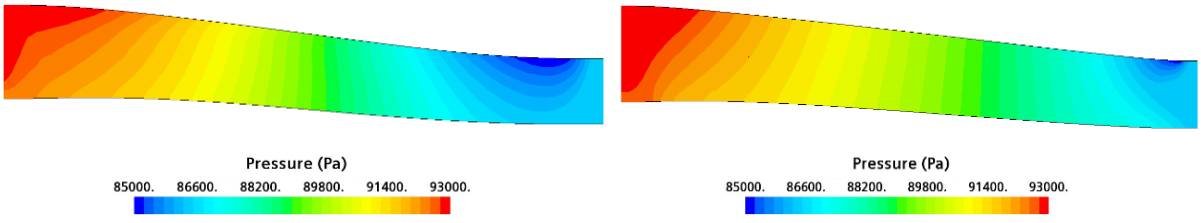

(**a**) (**b**)

Figure 36 Comparison of absolute pressure contour inside the duct in the xy plane, (**a**) the baseline geometry and (**b**) the optimized geometry

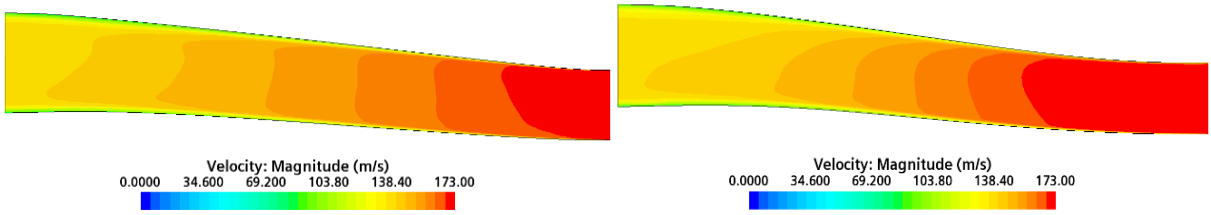

(**a**) (**b**)

Figure 37 Comparison of flow velocity inside the duct in the xy plane, (**a**) the baseline geometry and (**b**) the optimized geometry

6 Conclusion

Figure (37) shows the contour of the flow velocity inside the duct in the xy plane for two baseline geometry and optimized geometry states. According to the figure, the optimized velocity distribution in different sections is more uniform, reducing the flow turbulence at the duct outlet. Additionally, in the optimized geometry, the boundary layer thickness of the velocity has decreased, which means an increase in duct efficiency.

This research aimed to enhance the geometry of an engine inlet duct to minimize total pressure loss and flow distortion at its outlet plane. To accomplish this, a genetic algorithm was utilized as it is a metaheuristic algorithm well-suited for optimizing non-linear problems. It should be noted that the relationship between the inlet duct geometry and the parameters of total pressure loss and flow distortion is highly non-linear. In the validation stage, an optimized geometry was obtained that achieved the required accuracy. This resulted in a total pressure loss value of 0.0074 and a flow distortion value of 0.0078. These results represent a significant reduction in flow distortion and total pressure loss compared to the baseline geometry values of 0.0315 for flow distortion and 0.0089 for total pressure loss. The research has achieved its objectives, as demonstrated by the reduction in flow distortion and total pressure loss values.

References

[1] J. R. Weske, "*Pressure Loss in Ducts with Compound Elbows*," February 1943 as Advance Restricted Report, No. NACA-WR-W-39, National Advisory Committee for Aeronautics (NACA), Washington, 1943, USA, 19930093515.pdf.

[2] S. Wellborn, B. Reichert, and T. Okiishi, "An Experimental Investigation of the Flow in a Diffusing S-duct," in *28th Joint Propulsion Conference and Exhibit*, pp. 3622, 06 July 1992 - 08 July 1992, Nashville, TN, USA, https://doi.org/10.2514/6.1992-3622.

[3] A.-L. Delot, and R. Scharnhorst, "A Comparison of Several CFD Codes with Experimental Data in a Diffusing S-duct," in *49th AIAA/ASME/SAE/ASEE Joint Propulsion Conference*, pp. 3796, July 14 - 17, 2013, San Jose, CA, https://doi.org/10.2514/6.2013-3796.

[4] C. Fiola, and R. K. Agarwal, "Simulation of Secondary and Separated Flow in a Diffusing S-duct using Four Different Turbulence Models," *Proceedings of the Institution of Mechanical Engineers*, *Part G: Journal of Aerospace Engineering*, Vol. 228, No. 11, pp. 1954-1963, 2014, https://doi.org/10.1177/0954410013507249.

[5] C. Chiang, D. Koo, and D. W. Zingg, "Aerodynamic Shape Optimization of an S-duct Intake for a Boundary-layer Ingesting Engine," *Journal of Aircraft*, Vol. 59, No. 3, pp. 725-741, 2022, 10.2514/1.c036632.

[6] S. Ghosh, D. Pratihar, B. Maiti, and P. Das, "An Evolutionary Optimization of Diffuser Shapes Based on CFD Simulations," *International Journal for Numerical Methods in Fluids*, Vol. 63, No. 10, pp. 1147-1166, 2010, https://doi.org/10.1016/j.ijthermalsci.2010.106226.

[7] J. E. Hicken, and D. W. Zingg, "Aerodynamic Optimization Algorithm with Integrated Geometry Parameterization and Mesh Movement," *AIAA Journal*, Vol. 48, No. 2, pp. 400-413, 2010, https://doi.org/10.2514/1.44033.

[8] E. Immonen, "Shape Optimization of Annular S-ducts by CFD and High-order Polynomial Response Surfaces," *Engineering Computations*, Vol. 35, No. 2, pp. 932-954, 2018, https://doi.org/10.1108/EC-08-2017-0327.

[9] E. Manca, "Unsteady Aerodynamic Investigation of the Flow within an Optimized S-duct Intake," *MSc Thesis*, Cranfield University, UK, 2016.

[10] L. Zeng, D. Pan, S. Ye, and X. Shao, "A Fast Multiobjective Optimization Approach to S-duct Scoop Inlets Design with Both Inflow and Outflow," *Proceedings of the Institution of Mechanical Engineers, Part G: Journal of Aerospace Engineering*, Vol. 233, No. 9, pp. 3381-3394, 2019, https://doi.org/10.1177/0954410018795806.

[11] H. Parhrizkar, K. K. Aminjan, M. M. Doustdar, and A. Heydari, "Optimization of S-shaped Air Intake by Computational Fluid Dynamics," *International Journal of Fluid Mechanics & Thermal Sciences*, Vol. 5, No. 2, pp. 36, 2019, https://www.researchgate.net/publication/358898524.

[12] F. Furlan, N. Chiereghin, T. Kipouros, E. Benini, and M. Savill, "Computational Design of S-duct Intakes for Distributed Propulsion," *Aircraft Engineering and Aerospace Technology: an International Journal*, Vol. 86, No. 6, pp. 473-477, 2014, https://doi.org/10.1108/AEAT-04-2014-0046.

[13] R. Tridello, "Comparison of Genetic and Tabu Search Algorithms in Aerodynamic Design of S-ducts," *Master's Thesis*, Master's Degree in Aerospace Engineering, Department of Industrial Engineering DII, University of Padova, Italy, 14 Jul. 2017, https://hdl.handle.net/20.500.12608/27573.

[14] A. Rigobello, "A Multi-objective Shape Optimization of an S-duct Intake through NSGA-II Genetic Algorithm," *Master's Degree Course in Aerospace Engineering*, Department of Industrial Engineering DII, University of Padova, Italy, 2016, https://hdl.handle.net/20.500.12608/24630.

[15] N. Chiereghin L, Guglielmi, M. Savill, T, Kipouros, E. Manca, A. Rigobello, M. Barison and E. Benini "Shape Optimization of a Curved Duct with Free form Deformations," in *23rd AIAA Computational Fluid Dynamics Conference*, pp. 4114, Denver, Colorado, USA, 2017, https://doi.org/10.2514/6.2017-4114.

[16] A. D'ambros, T. Kipouros, P. Zachos, M. Savill, and E. Benini, "Computational Design Optimization for S-ducts," *Designs*, Vol. 2, No. 4, pp. 36, 2018, https://doi.org/10.3390/designs2040036.

[17] W. Gan and X. Zhang, "Design Optimization of a Three-dimensional Diffusing S-duct using a Modified SST Turbulent Model," *Aerospace Science and Technology*, Vol. 63, pp. 63-72, 2017, https://doi.org/10.1016/j.ast.2016.12.016.

[18] A. Meneghin, "Three-objective Optimization Studies of an S-duct," *MSc Thesis*, Department of Industrial Engineering, MSc in Aerospace Engineering, University of Padova, Italy, 2020, https://hdl.handle.net/20.500.12608/21111.

[19] V. Kamat, V. Rao, M. Xu, and S. Saxena, "Flow Distortion Based S-duct Optimization using Adjoint Methodology," in *AIAA Aviation 2020 Forum*, pp. 2755, 2020, https://doi.org/10.2514/6.2020-2755.

[20] S. Sadatpour, A. Madadi, and R. Ahadian, "Numerical Optimization of S-shaped Intake Performance using Special Cross-sectional Profiles," *Thermophysics and Aeromechanics*, Vol. 29, No. 5, pp. 689-702, 2022, https://doi.org/10.1134/S0869864322050079.